Reactivity of cobalt(II)-dichalcogenide complexes: correlation between redox conversion and ligand-field strength

Marvelous, C.

Appendix I

Supplementary Information for Chapter 2

Synthesis of Compound $[Co(L^1S)(phen)](SbF_6)_2$

The compound $[Co(L^1S)(phen)](SbF_6)_2$ was prepared in a similar manner as compound [**3**]$(SbF_6)_2$, using 1,10-phenanthroline (phen) instead of bpy. A red powder was obtained in 85% yield. IR (neat, cm^{-1}): 1608s, 1518m, 1485w, 1426s, 1376w, 1344w, 1298w, 1247w, 1225w, 1149w, 1105m, 1091m, 1058m, 1022m, 979w, 955w, 909w, 869w, 847s, 769s, 726s, 649vs, 569m, 526m, 448m, 421s. ESI-MS in acetonitrile calcd. for $[Co(L^1S)(phen)](SbF_6)^+$ *m/z* 732.0, found *m/z* 732.0; calcd. for $[Co(L^1S)(phen)]^{2+}$ *m/z* 248.55, found m/z 248.6; calcd. for $[Co(phen)_3]^{2+}$ *m/z* 299.6, found *m/z* 299.9. Elemental analysis (%) for $[Co(L^1S)(phen)](SbF_6)_2$, calcd. C, 32.23; H, 2.50; N, 7.23; found C, 33.03; H, 2.48; N, 7.18. Single crystals were obtained by vapor diffusion of dry and deoxygenated diethyl ether into the dry and deoxygenated acetonitrile solution of compound $[Co(L^1S)(phen)](SbF_6)_2$.

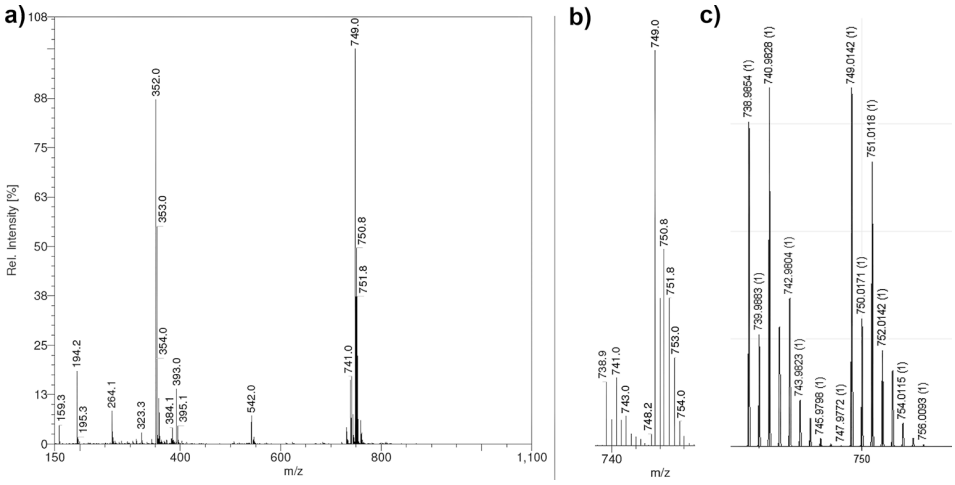

Figure AI.1. ESI-MS spectrum of a) [$\mathbf{1}_{Cl}$] dissolved in acetonitrile; b) the experimental isotopic distribution of the main signals; c) simulated isotopic distribution of the main signals. ESI-MS found (calcd.) for $[\mathbf{1}_{Cl} - 2Cl^-]^{2+}$ *m/z* 352.0 (352.0), for $[\mathbf{1}_{Cl} - Cl^-]^+$ *m/z* 741.0 (741.0), and for $[\mathbf{1}_{Cl} - 2Cl^- + HCOO^-]^+$ *m/z* 749.0 (749.0).

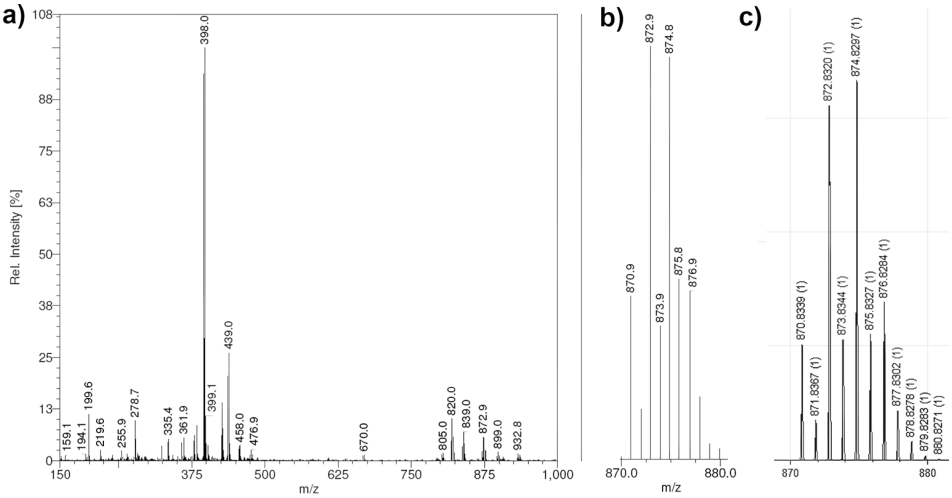

Figure AI.2. ESI-MS spectrum of a) [$\mathbf{1}_{\mathbf{Br}}$] dissolved in acetonitrile; b) the experimental isotopic distribution; c) simulated isotopic distribution. ESI-MS found (calcd.) for $[\mathbf{1}_{\mathbf{Br}} - 2Br^-]^{2+}$ *m/z* 398.0 (397.9), for $[\mathbf{1}_{\mathbf{Br}} - 2Br^- + HCOO^-]^+$ *m/z* 839.0 (838.9), and for $[\mathbf{1}_{\mathbf{Br}} - Br^-]^+$ *m/z* 872.9 (872.8).

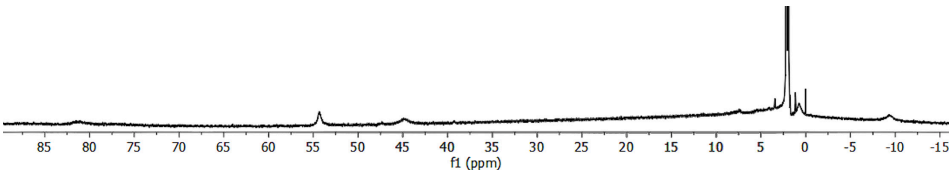

Figure AI.3. ^{1}H-NMR spectrum of compound [$\mathbf{1}_{\mathbf{Cl}}$] dissolved in CD_3CN.

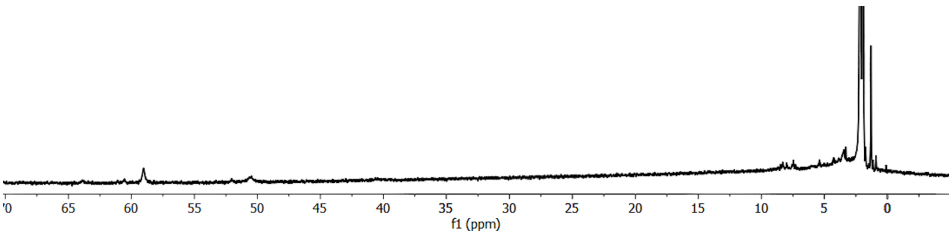

Figure AI.4. ^{1}H-NMR spectrum of compound [$\mathbf{1}_{\mathbf{Br}}$] dissolved in CD_3CN.

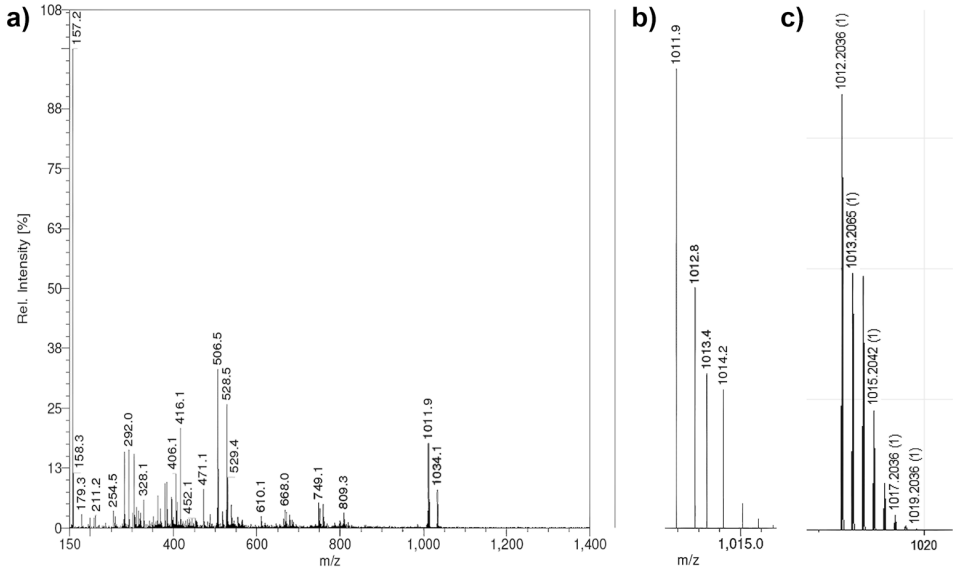

Figure AI.5. ESI-MS spectrum of a) [**2**$_{Cl}$](BPh$_4$)$_2$ dissolved in methanol; b) the experimental isotopic distribution; c) simulated isotopic distribution. ESI-MS found (calcd.) for [**2**$_{Cl}$ – Cl^- + OMe^-]$^{2+}$ *m/z* 506.5 (506.1), for partially reduced species [**2**$_{Cl}$ – Cl^- + OMe^-]$^+$ *m/z* 1011.9 (1012.2).

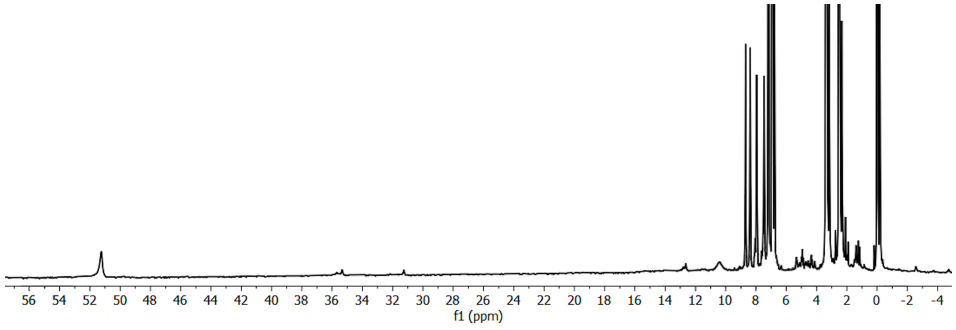

Figure AI.6. ^{1}H-NMR spectrum of compound [**2**$_{Cl}$](BPh$_4$)$_2$ dissolved in DMSO-d$_6$. The diamagnetic region contains peaks that corresponds to the ligand L^1SSL^1 and bipyridine, indicating dissociation of the ligand upon dissolution of the compound.

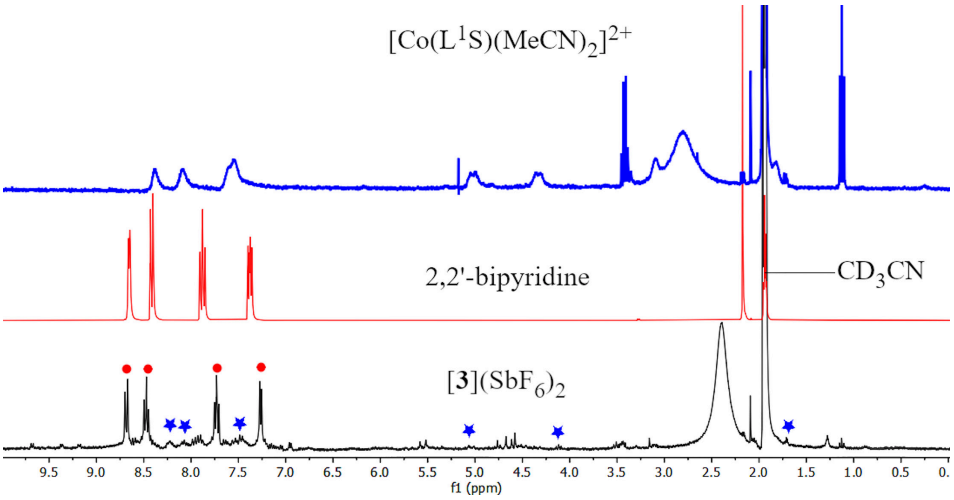

Figure AI.7. ^{1}H-NMR spectrum of compound [**3**](SbF$_6$)$_2$ (black trace) dissolved in CD$_3$CN. ^{1}H-NMR spectrum of [Co(L^{1}S)(MeCN)$_2$]$^{2+}$ (blue trace) and 2,2'-bipyridine (red trace) dissolved in CD$_3$CN are provided. The red dots and blue stars indicated the presence of 2,2'-bipyridine and [Co(L^{1}S)(MeCN)$_2$]$^{2+}$, respectively.

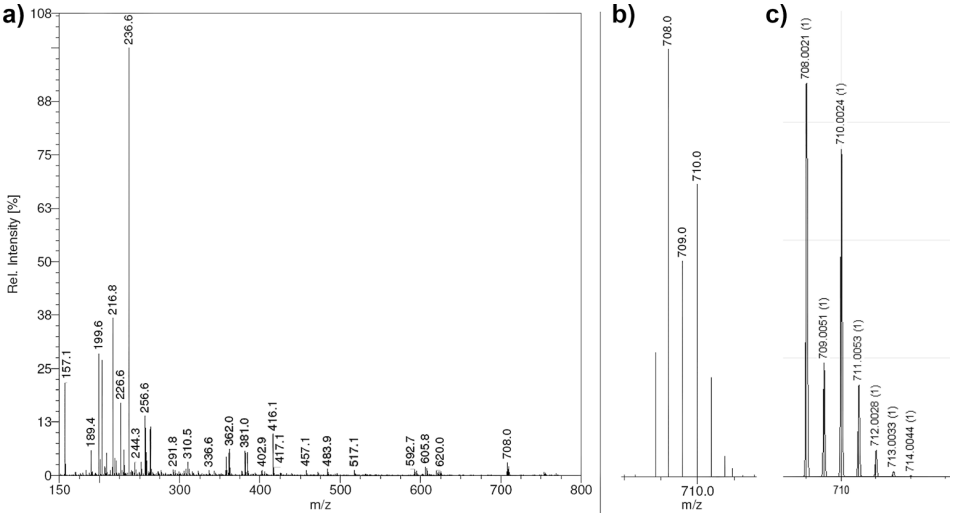

Figure AI.8. ESI-MS spectrum of a) [**3**](SbF$_6$)$_2$ dissolved in acetonitrile; b) the experimental isotopic distribution; c) simulated isotopic distribution. ESI-MS found (calcd.) for [**3**]$^{2+}$ *m/z* 236.6 (236.55), for [**3**](SbF$_6$)$^{+}$ *m/z* 708.0 (708.0). Species [Co(L^{1}S)(MeCN)$_2$]$^{2+}$ (*m/z* 199.6 (199.55)) and [2,2'-bipyridine + H]$^{+}$ (*m/z* 157.1 (157.0)) are present.

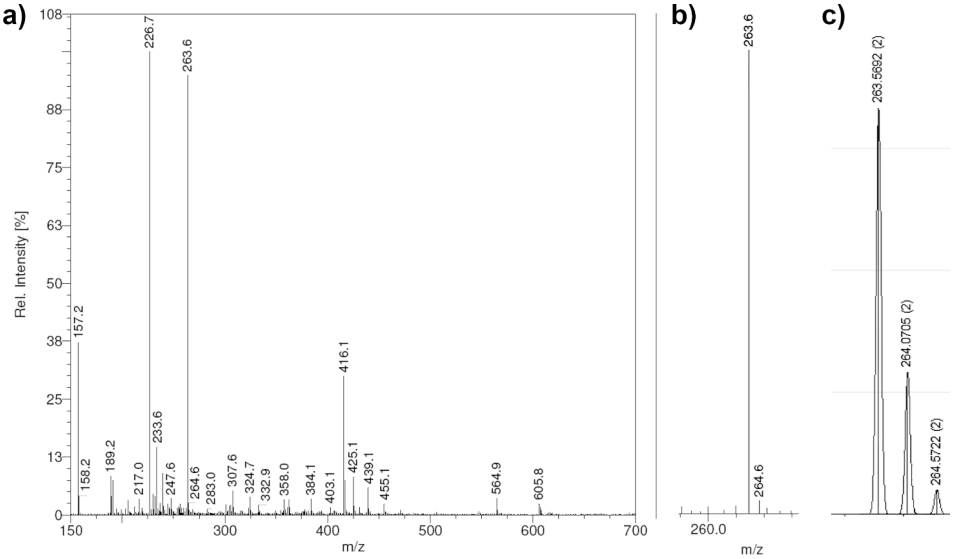

Figure AI.9. ESI-MS spectrum of a) the isolated brown-reddish powder from the reaction between [**2**$_{Cl}$](BPh$_4$)$_2$ with AgSbF$_6$, the powder was dissolved in acetonitrile; b) the experimental isotopic distribution; c) simulated isotopic distribution. ESI-MS found (calcd.) for $[(Co(bpy)_3]^{2+}$ *m/z* 263.6 (263.6).

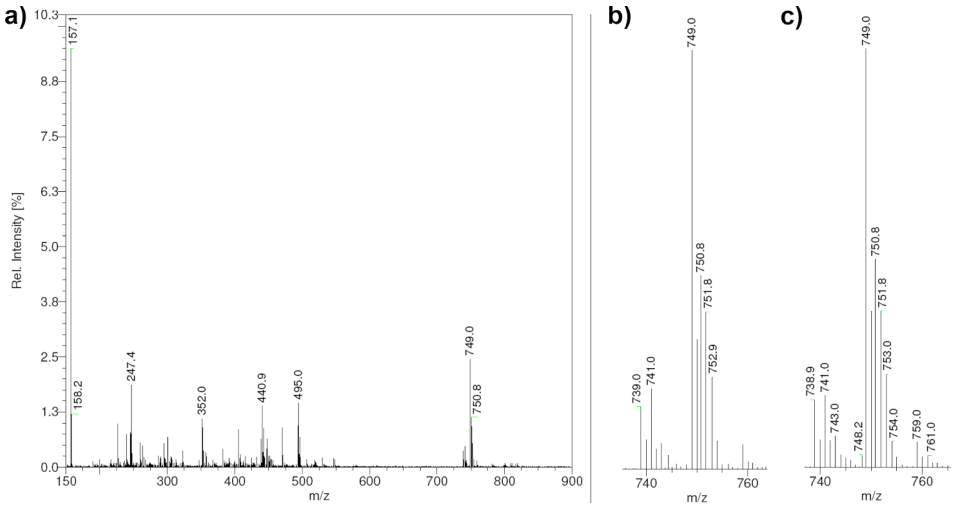

Figure AI.10. ESI-MS spectrum of a) the isolated purple powder from the reaction between [**3**](SbF$_6$)$_2$ with NEt$_4$Cl, the powder was dissolved in acetonitrile; b) the experimental isotopic distribution; c) the experimental isotopic distribution for compound [**1**$_{Cl}$]. ESI-MS found (calcd.) for $[\mathbf{1}_{Cl} - 2Cl^-]^{2+}$ *m/z* 352.0 (352.0), for $[\mathbf{1}_{Cl} - Cl^-]^+$ *m/z* 741.0 (741.0), and for $[\mathbf{1}_{Cl} - 2Cl^- + HCOO^-]^+$ *m/z* 749.0 (749.0).

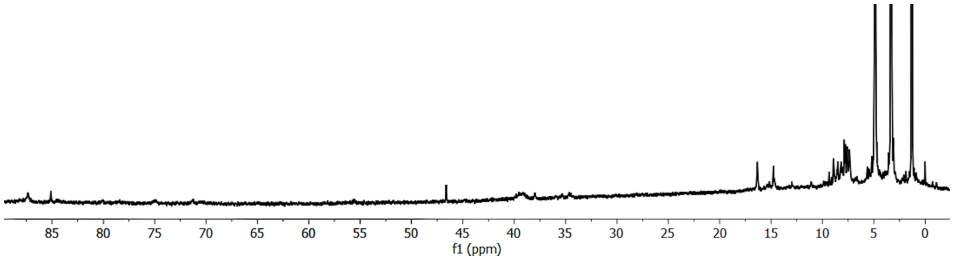

Figure AI.11. ^{1}H-NMR spectrum of the isolated purple powder from the reaction between [**3**](SbF$_6$)$_2$ with NEt$_4$Cl, the powder was dissolved in CD$_3$CN.

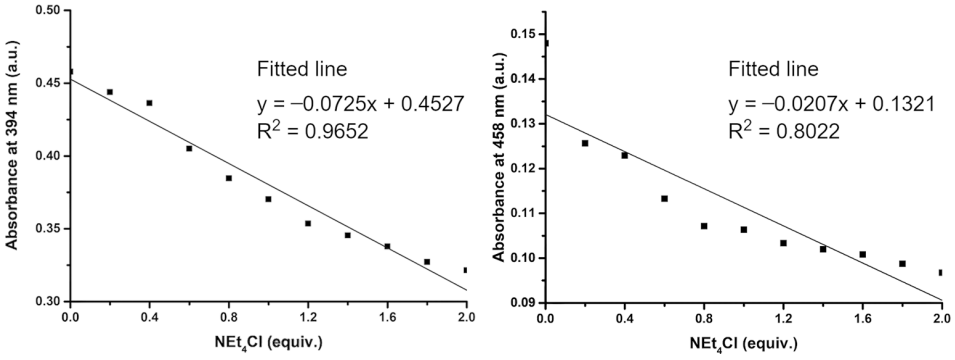

Figure AI.12. Changes of absorbance at 394 nm and 458 nm as a function of the amount of added NEt$_4$Cl to 5 mM solution of [**3**](SbF$_6$)$_2$. Linear fitting details are provided.

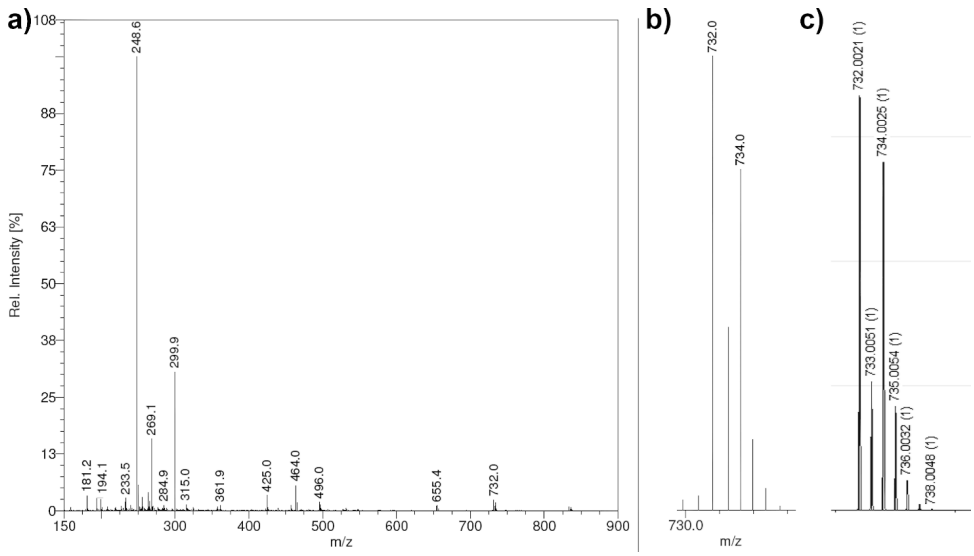

Figure AI.13. ESI-MS spectrum of a) $[Co(L^1S)(phen)](SbF_6)_2$, the powder was dissolved in acetonitrile; b) the experimental isotopic distribution; c) simulated isotopic distribution. ESI-MS found (calcd.) for $[Co(L^1S)(phen)]^{2+}$ *m/z* 248.6 (248.55) and for $[Co(L^1S)(phen)](SbF_6)^+$ *m/z* 732.0 (732.0). The species $[Co(phen)_3]^{2+}$ is also found (calcd.) at *m/z* 299.9 (299.6).

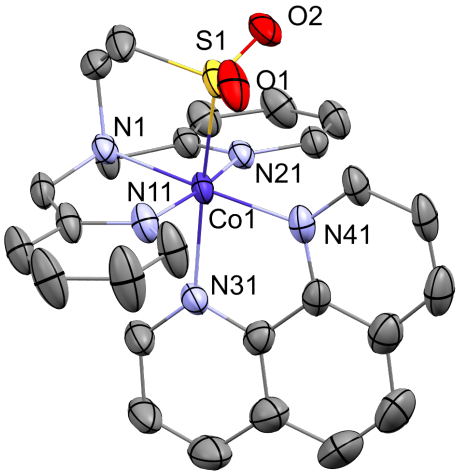

Figure AI.14. Displacements ellipsoid plot (50% probability level) of the oxidized compound $[Co(L^1SO_2)(phen)](SbF_6)_2$ at 110(2) K. Hydrogen atoms, non-coordinated anions, and lattice solvent molecules are omitted for clarity.

Table AI.1. Selected bond distances and bond angles in $[Co(L^1SO_2)(phen)](SbF_6)_2$.

Atoms	distance (Å)	Atoms	Bond angles (°)
Co1–N1	1.976(4)	S1−Co1−N1	86.78(11)
Co1–N11	1.921(4)	S1−Co1−N11	88.59(13)
Co1–N21	1.929(4)	S1−Co1−N21	95.64(11)
Co1–N31	2.084(4)	S1−Co1−N31	172.01(12)
Co1–N41	1.969(4)	S1−Co1−N41	92.32(12)
Co1–S1	2.1866(13)	N31−Co1−N41	82.36(16)
S1–O1	1.460(4)	N31−Co1−N1	98.77(15)
S1–O2	1.456(4)	N21−Co1−N1	84.00(16)

Table AI.2. Crystallographic Data for the crystal structures in the present work.

	[$\mathbf{1}_{Br}$]	[$\mathbf{2}_{Cl}$](BPh$_4$)$_2$	[Co(L^{1}SO$_2$)(phen)](SbF$_6$)$_2$
Chemical formula	$C_{28}H_{32}Br_4Co_2N_6S_2$, CH_4O	$C_{48}H_{48}Cl_2Co_2N_{10}S_2$, 2($C_{24}H_{20}B$), 2($C_3H_6O$), 0.42(O)	$C_{26}H_{24}CoN_5O_2S$, 2(F_6Sb), 0.566($C_4H_{10}O$), 1.434(C_2H_3N)
M_r	986.26	1779.17	1101.82
Crystal system	Monoclinic	Monoclinic	Monoclinic
Space group	$P2_1/c$	$C2/c$	$P2_1/c$
Cell lengths (*a, b, c*) (Å)	15.7651(7), 11.9665(5), 19.6343(8)	19.0139(7), 20.1121(7), 27.0156(13)	21.5627 (5), 13.6523 (4), 14.0315 (4)
Cell angles (α, β, γ) (°)	90, 103.345(4), 90	90, 108.171(4), 90	90, 103.059 (3), 90
Cell volume (Å^3)	3604.1 (3)	9815.8 (7)	4023.8 (2)
Z	4	4	4
μ (mm^{-1})	5.50	0.49	1.89
Crystal size (mm)	0.11 × 0.08 × 0.02	0.26 × 0.19 × 0.10	0.29 × 0.09 × 0.05
Temperature (K)	110(2)	110(2)	110(2)
Diffractometer	SuperNova, Dual, Cu at zero, Atlas detector	SuperNova, Dual, Cu at zero, Atlas detector	SuperNova, Dual, Cu at zero, Atlas detector
Radiation type	Mo *K*α	Mo *K*α	Mo *K*α
T_{min}, T_{max}	0.734, 0.982	0.520, 1.000	0.439, 1.000
No. of measured, independent and observed [$I > 2\sigma(I)$] reflections	28658, 6355, 4720	38544, 11261, 8613	50549, 7091, 5615
R_{int}	0.065	0.038	0.049
$(\sin\theta/\lambda)_{max}$ (Å^{-1})	0.595	0.650	0.595
$R[F^2 > 2\sigma(F^2)]$, $wR(F^2)$, S	0.047, 0.114, 1.05	0.043, 0.105, 1.02	0.039, 0.102, 1.04
No. of reflections	6355	11261	7091
No. of parameters	398	652	661
No. of restraints		309	404
H-atom treatment	H-atom parameters constrained	H-atom parameters constrained	H-atom parameters constrained
$\Delta\rho_{max}$, $\Delta\rho_{min}$ (e Å^{-3})	1.94, -0.82	0.56, -0.31	0.79, -0.77

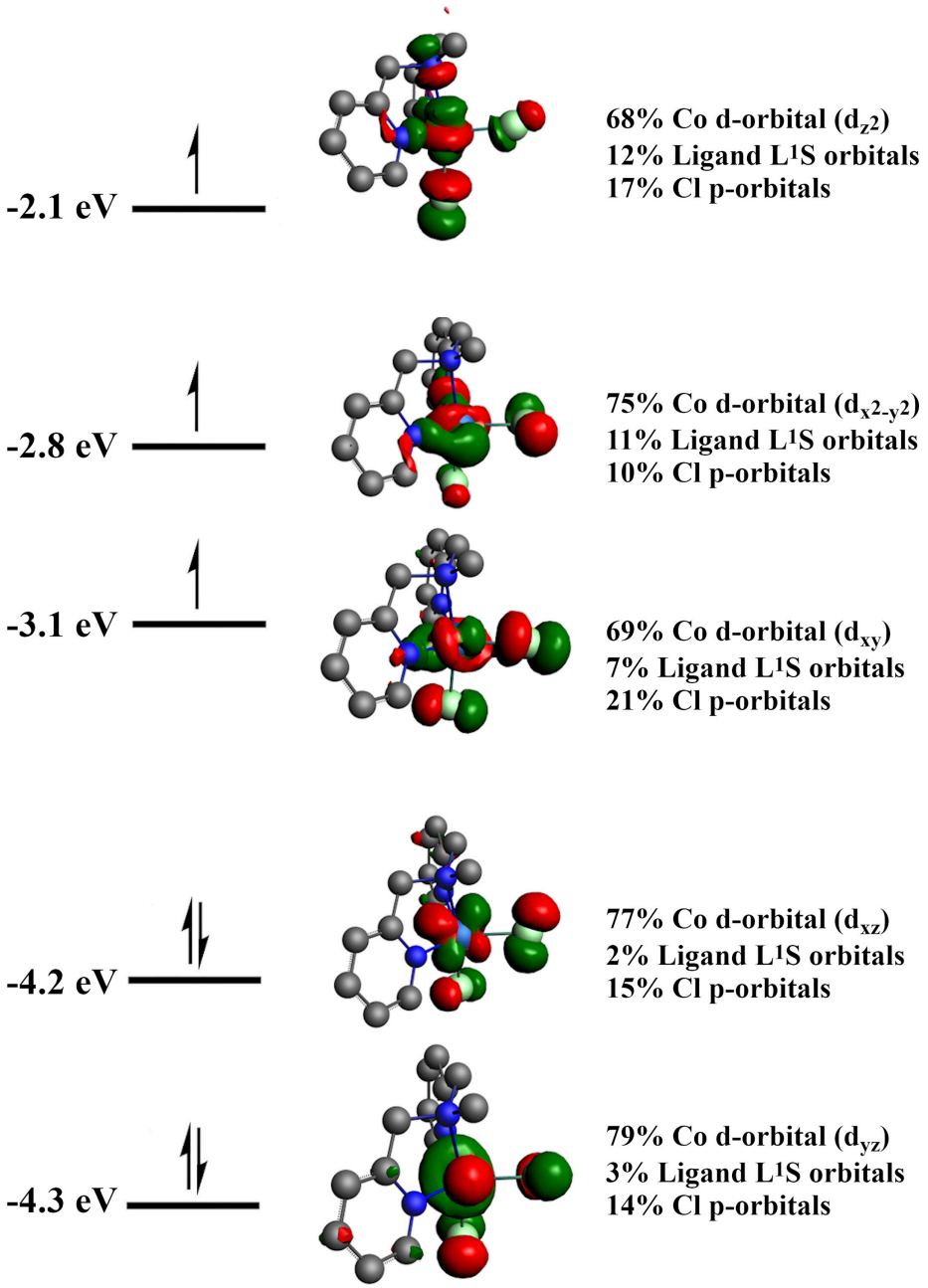

Figure AI.15. Several frontier orbitals of [**1***] associated with Co *d*-orbitals along with their energies, orbital visualization, and orbital composition.

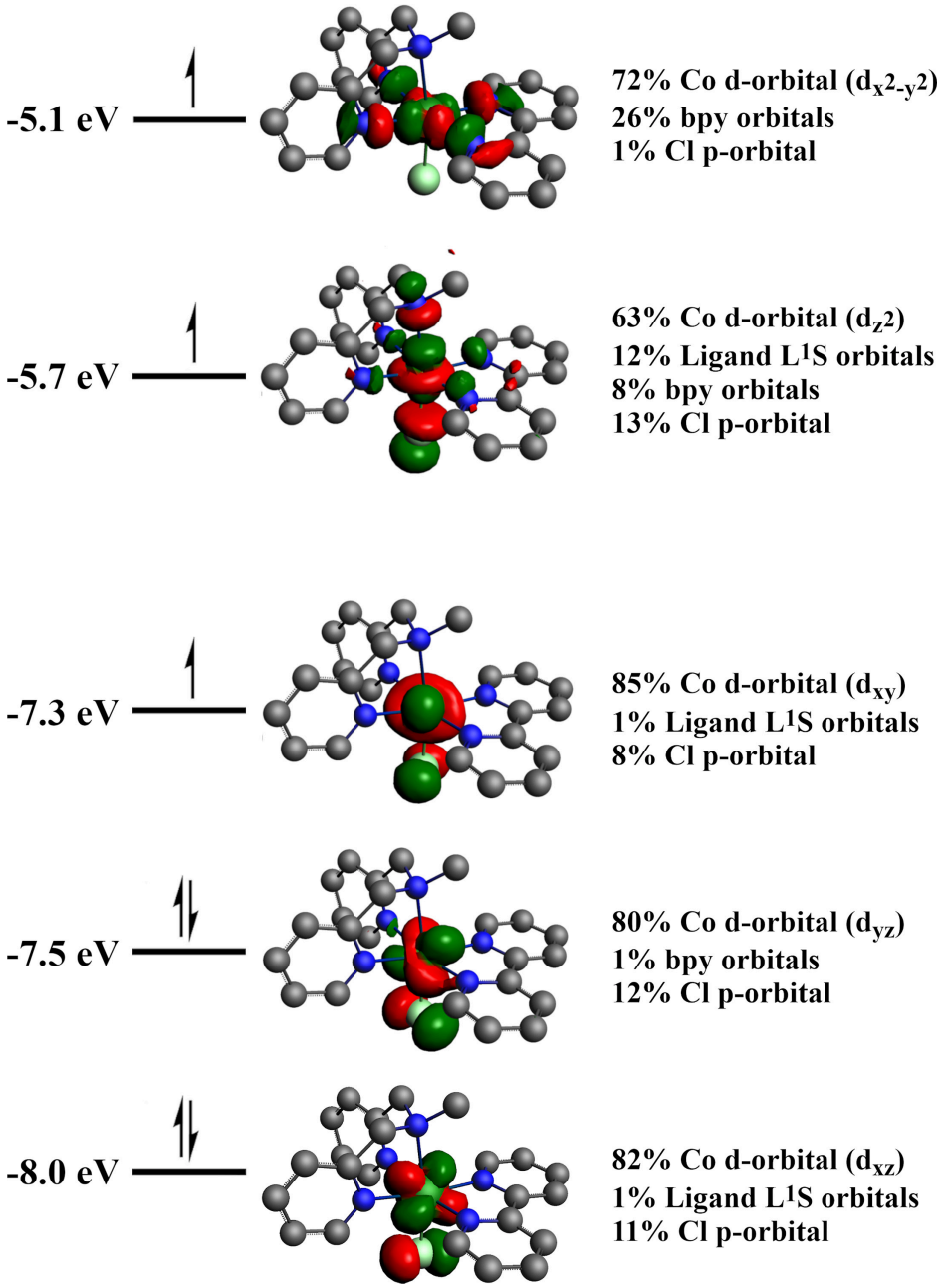

Figure AI.16. Several frontier orbitals of $[\mathbf{2^*}]^+_{fac}$ associated with Co *d*-orbitals along with their energies, orbital visualization, and orbital composition.

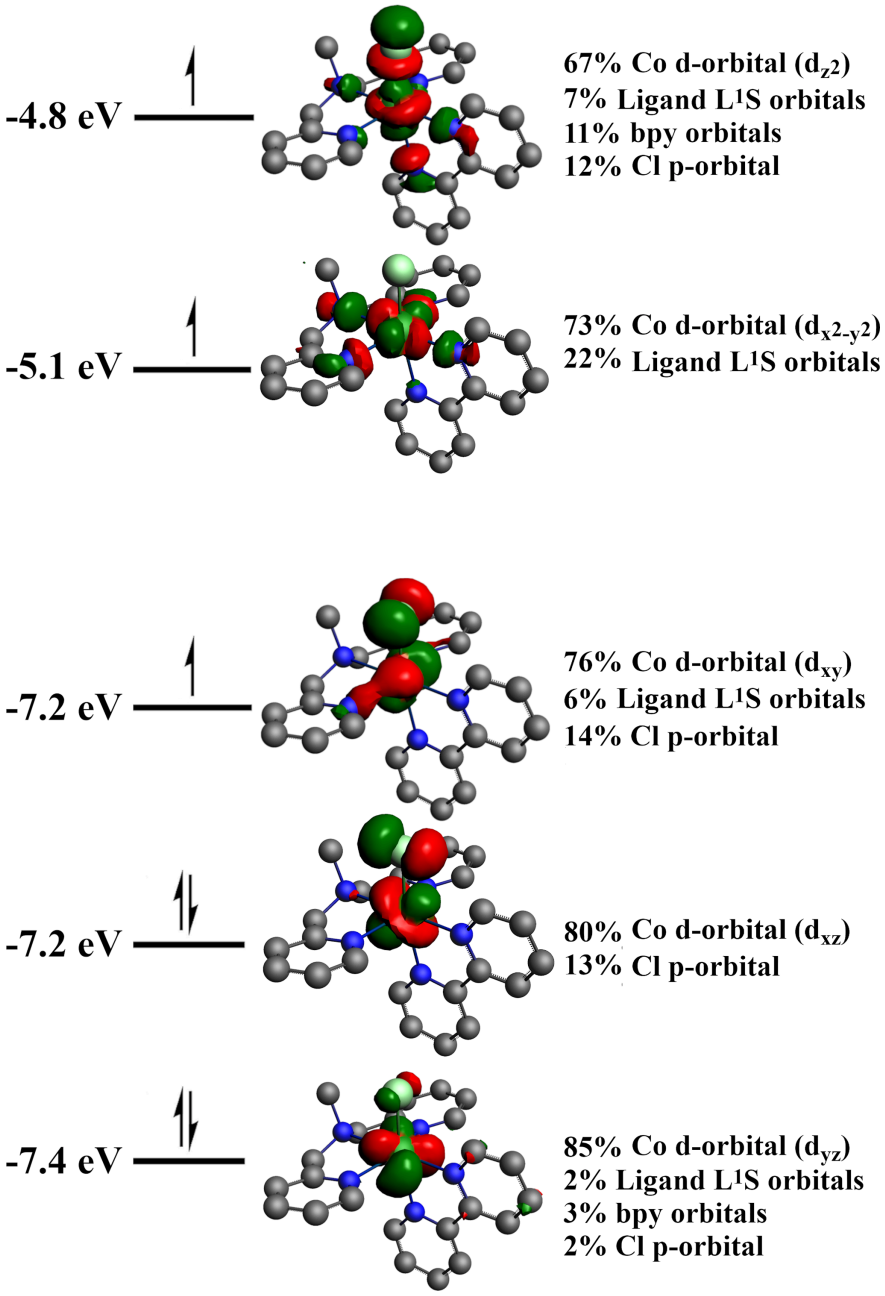

Figure AI.17. Several frontier orbitals of $[\mathbf{2^*}]^+_{mer}$ associated with Co *d*-orbitals along with their energies, orbital visualization, and orbital composition.

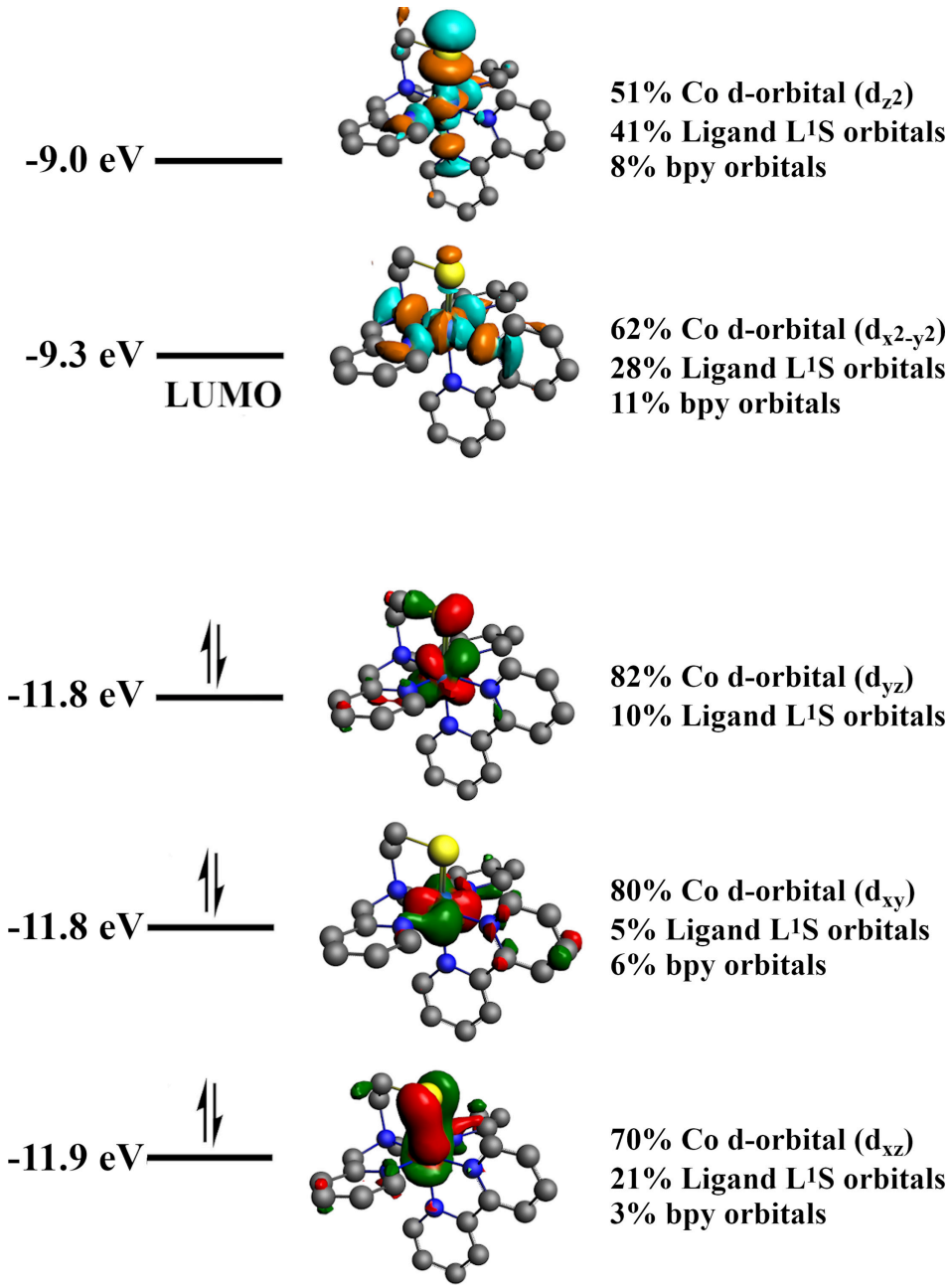

Figure AI.18. Several frontier orbitals of $[\mathbf{3}]^{2+}_{mer}$ associated with Co *d*-orbitals along with their energies, orbital visualization, and orbital composition.

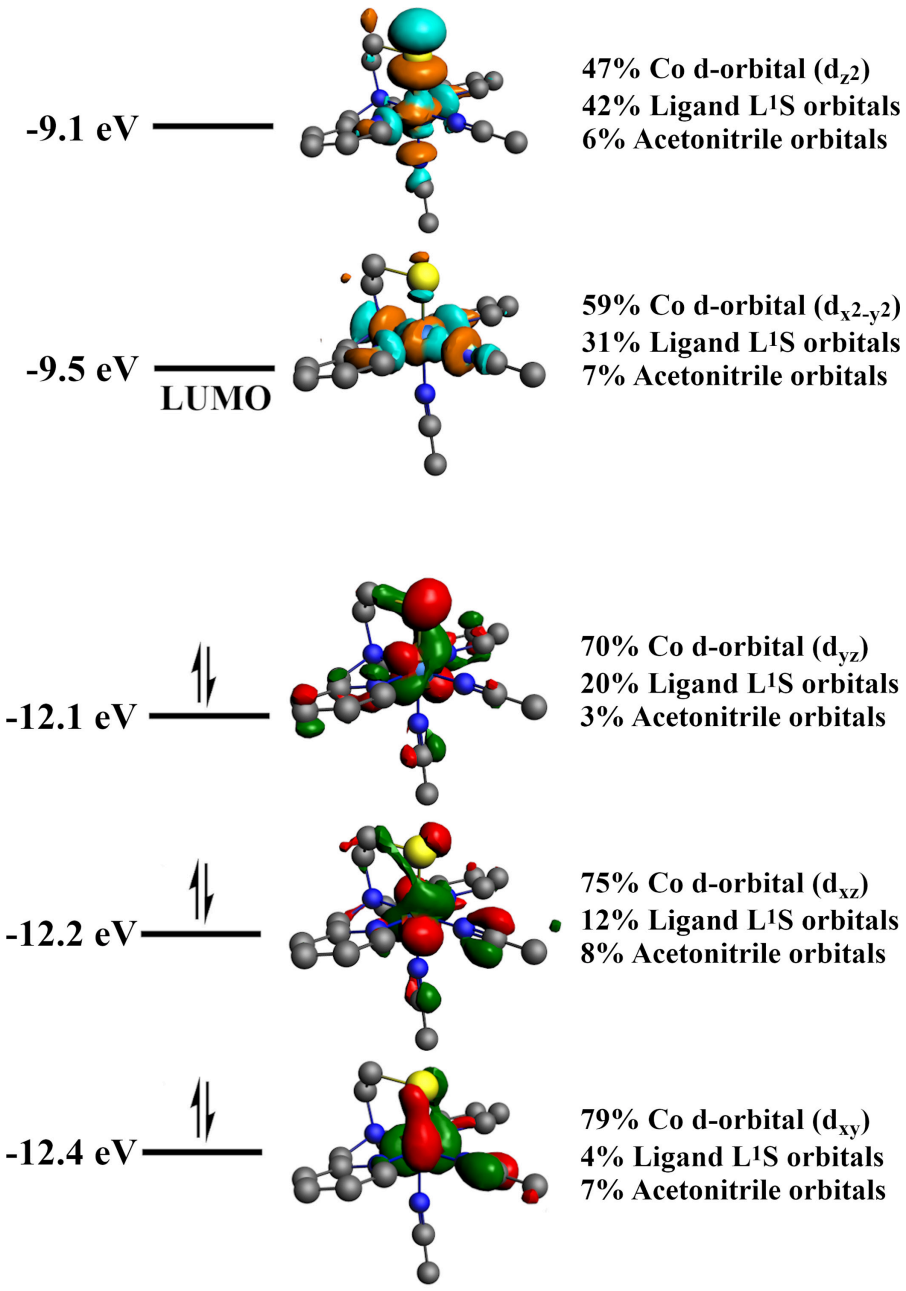

Figure AI.19. Several frontier orbitals of [**4**]$^{2+}$ associated with Co *d*-orbitals along with their energies, orbital visualization, and orbital composition.

Appendix II

Supplementary Information for Chapter 3

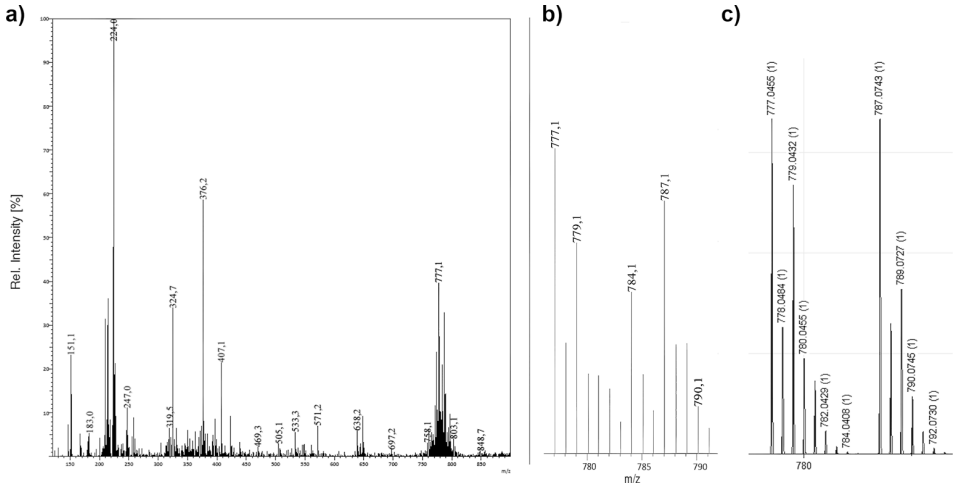

Figure AII.1. ESI−MS spectrum of compound [**2**$_{SS}$] dissolved in methanol. ESI−MS found (calcd.) for [**2**$_{SS}$ – 4Cl$^-$ + 2HCOO$^-$]$^{2+}$ *m/z* 376.2 (376.04), for [**2**$_{SS}$ – 2Cl$^-$ + HCOO$^-$]$^+$ *m/z* 777.1 (777.05), and for [**2**$_{SS}$ – 3Cl$^-$ + 2HCOO$^-$]$^+$ *m/z* 787.1 (787.07).

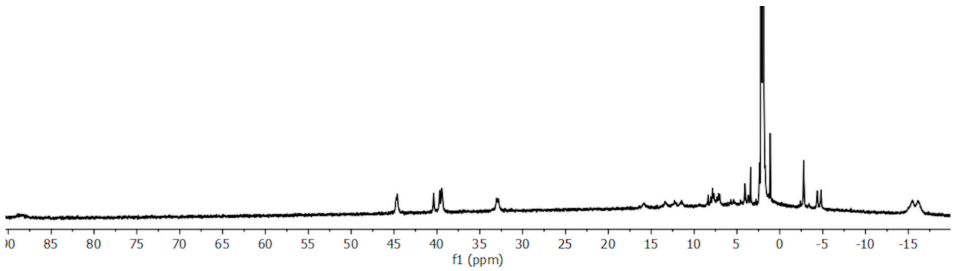

Figure AII.2. ^{1}H-NMR spectrum of compound [**2**$_{SS}$] dissolved in CD_3CN.

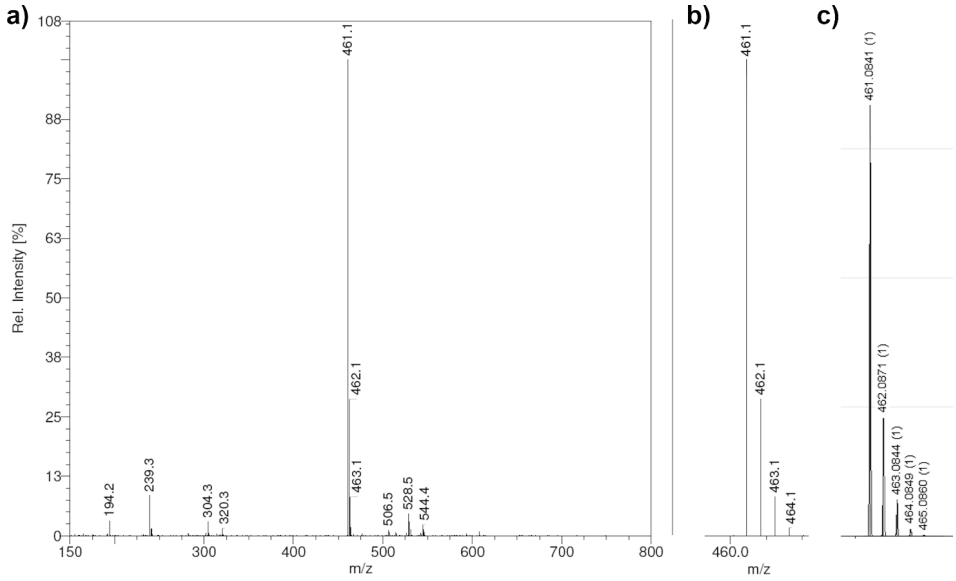

Figure AII.3. ESI−MS spectrum of a) [**1s**]Cl dissolved in methanol; b) the experimental isotopic distribution of the main signal; c) simulated isotopic distribution. ESI−MS found (calcd.) for $[\mathbf{1s}]^+$ *m/z* 461.1 (461.08).

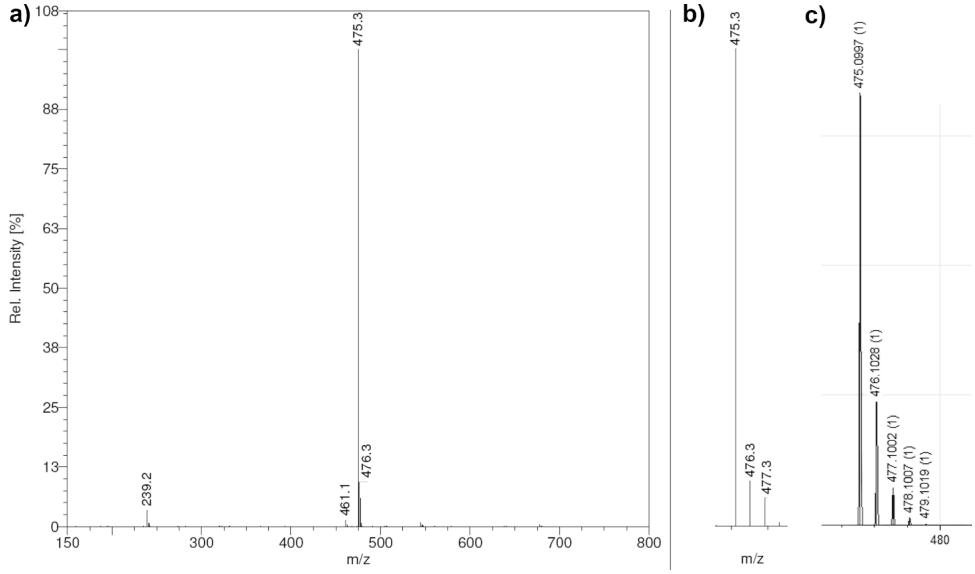

Figure AII.4. ESI−MS spectrum of a) [**2s**]Cl dissolved in acetonitrile; b) the experimental isotopic distribution of the main signal; c) simulated isotopic distribution. ESI−MS found (calcd.) for $[\mathbf{2s}]^+$ *m/z* 475.3 (475.1).

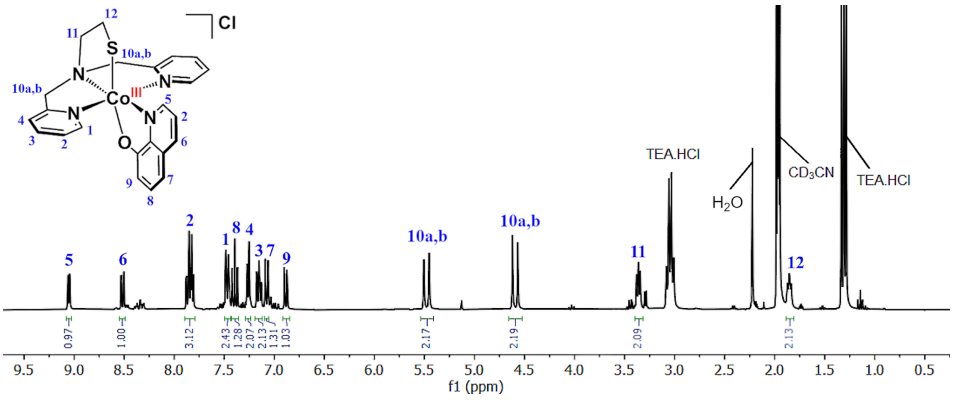

Figure AII.5. ^{1}H-NMR spectrum of [**1s**]Cl dissolved in CD_3CN.

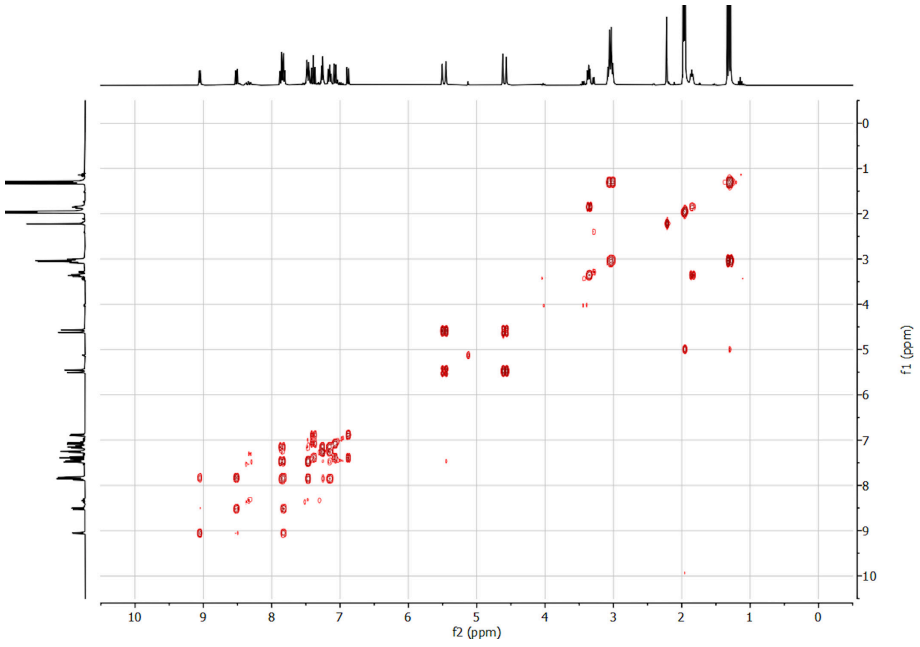

Figure AII.6. ^{1}H–^{1}H-COSY NMR spectrum of [**1s**]Cl dissolved in CD_3CN.

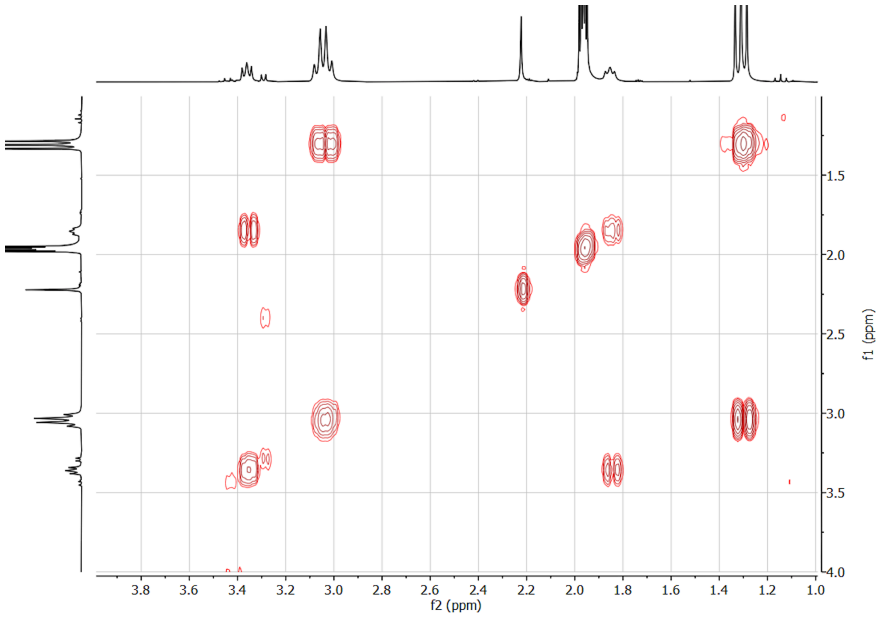

Figure AII.7. ^{1}H–^{1}H-COSY NMR spectrum of [**1s**]Cl dissolved in CD_3CN. The spectrum shows the correlation of protons in N-C**H**$_2$-C**H**$_2$-S (3.2–3.5 ppm and 1.84−1.87 ppm).

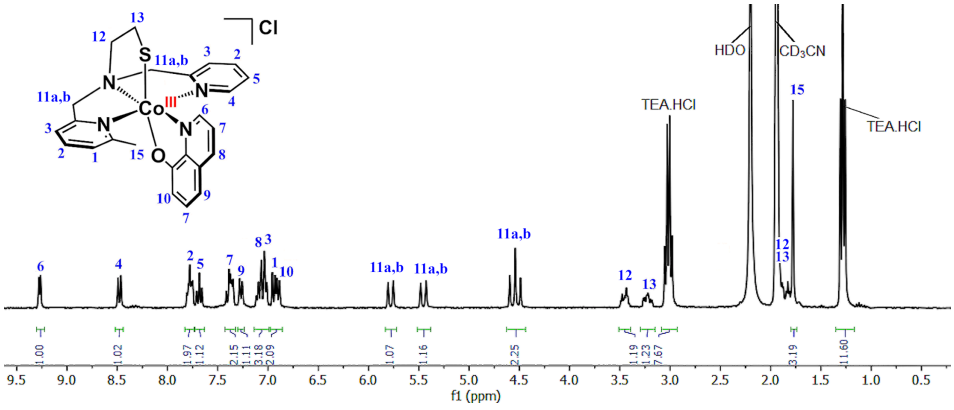

Figure AII.8. ^{1}H-NMR spectrum of [**2s**]Cl dissolved in CD_3CN.

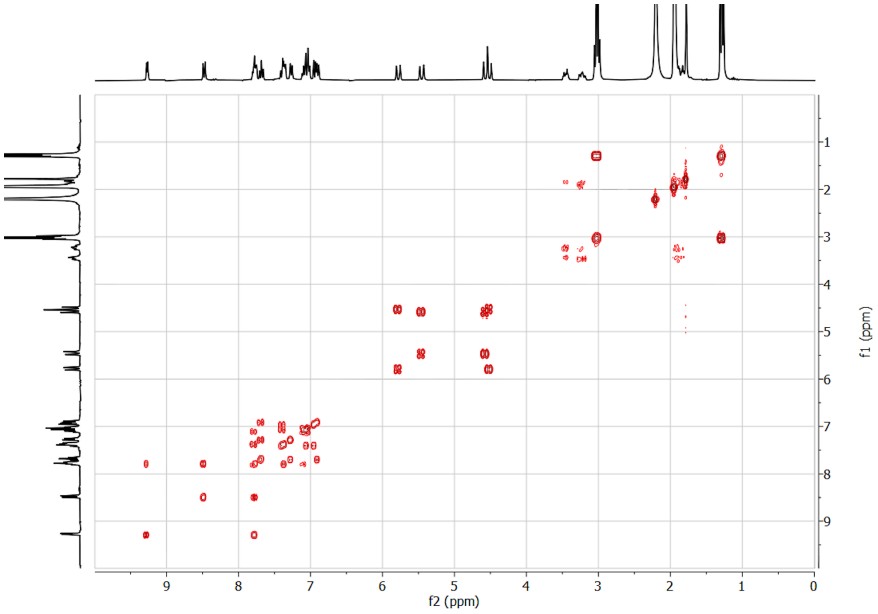

Figure AII.9. ^{1}H–^{1}H-COSY NMR spectrum of [**2s**]Cl dissolved in CD_3CN.

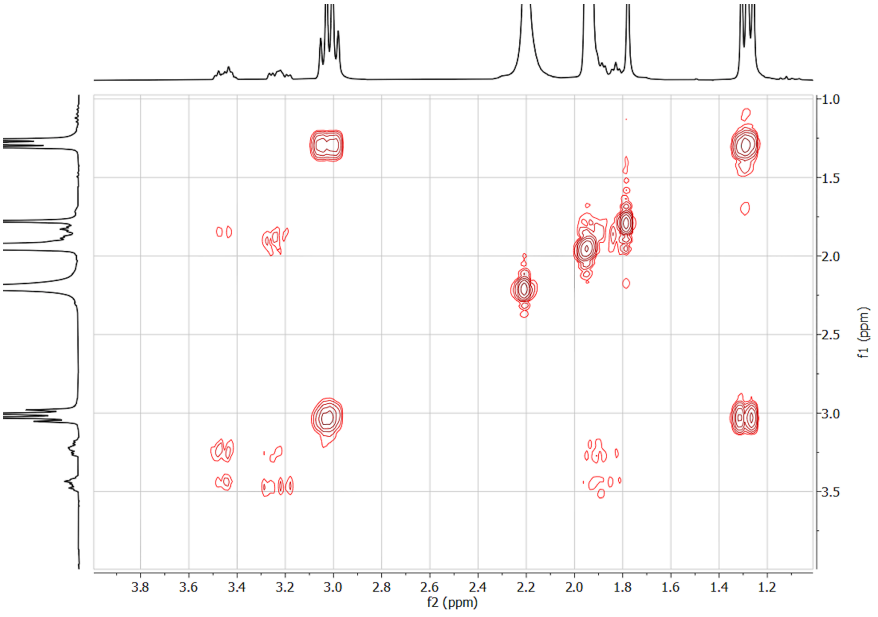

Figure AII.10. ^{1}H–^{1}H-COSY NMR spectrum of [**2s**]Cl dissolved in CD_3CN. The spectrum shows the correlation of protons in N-C**H**$_2$-C**H**$_2$-S (3.18–3.50 ppm) with the solvent peak (1.9 ppm), indicating that the solvent peak obscures the proton peak of interest.

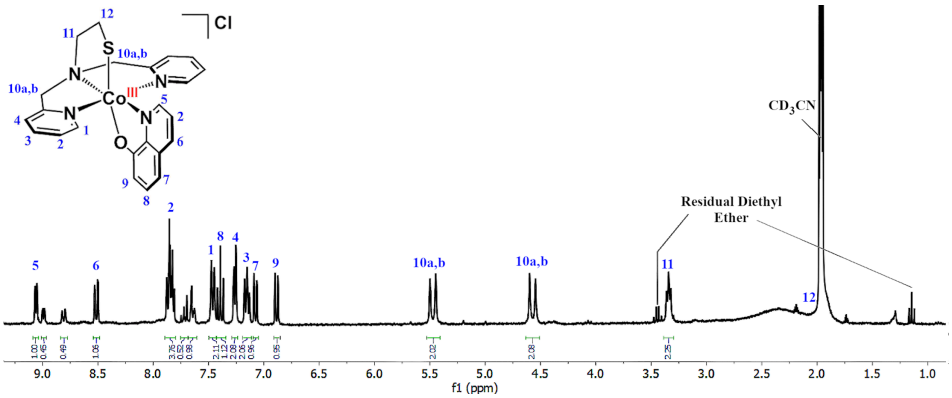

Figure AII.11. ^{1}H-NMR spectrum of [**1S**]Cl dissolved in CD_3CN. The synthesis was done in absence of triethylamine. Impurities (as unlabeled peaks) are present mostly in the aromatic region.

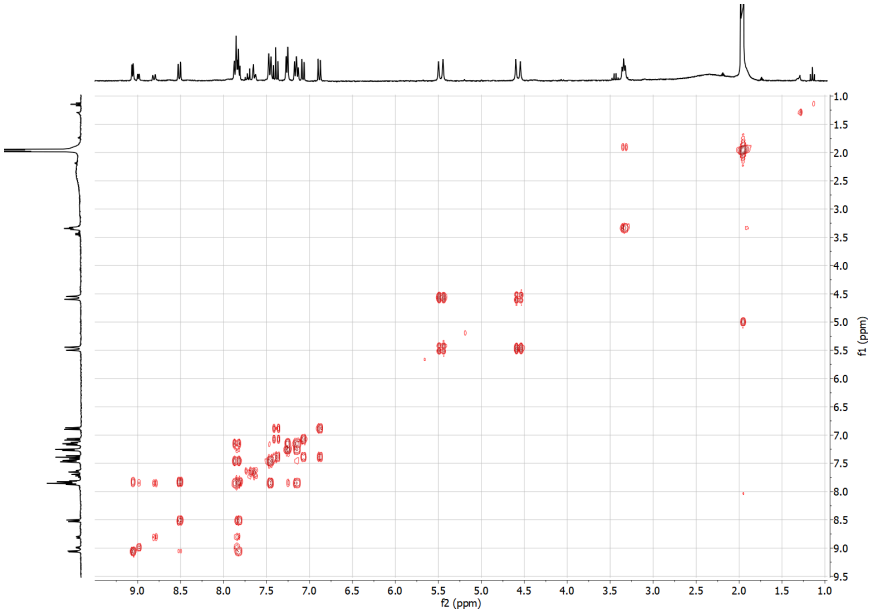

Figure AII.12. ^{1}H−^{1}H-COSY NMR spectrum of [**1S**]Cl dissolved in CD_3CN. The synthesis was done in absence of triethylamine.

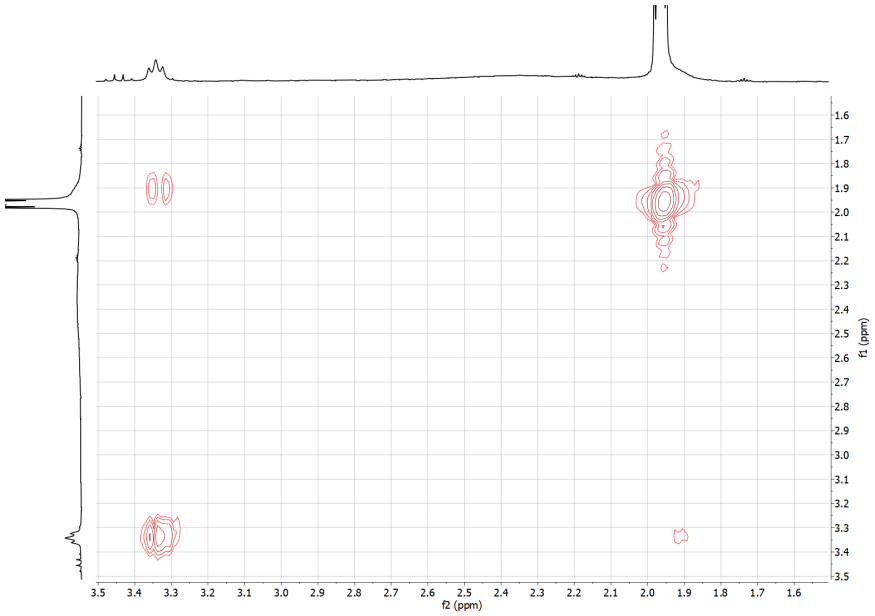

Figure AII.13. $^{1}H-^{1}H$-COSY NMR spectrum of [**1s**]Cl dissolved in CD_3CN. The synthesis was done in absence of triethylamine. The spectrum shows the correlation of protons in N-C**H₂**-C**H₂**-S (3.2–3.4 ppm and 1.84−1.87 ppm).

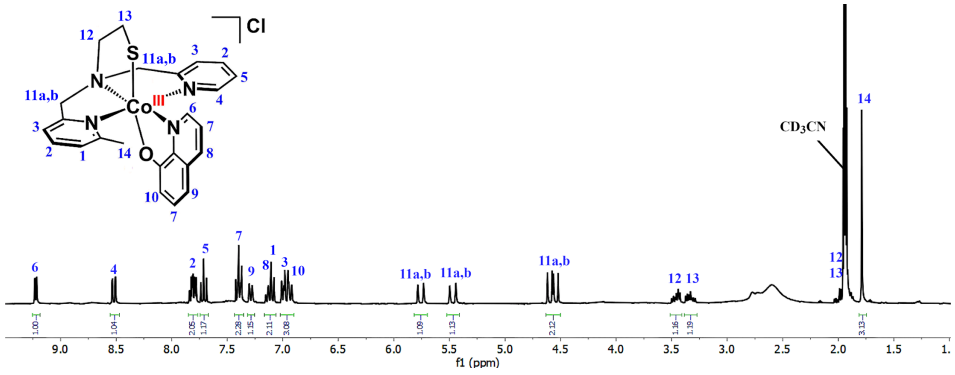

Figure AII.14. ^{1}H-NMR spectrum of [**2s**]Cl dissolved in CD_3CN. The synthesis was done in absence of triethylamine.

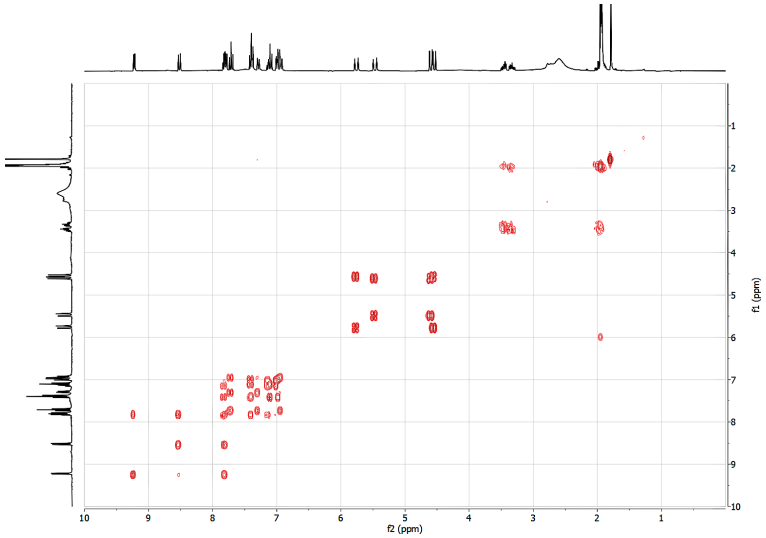

Figure AII.15. $^{1}H-^{1}H$-COSY NMR spectrum of [**2s**]Cl dissolved in CD_3CN. The synthesis was done in absence of triethylamine.

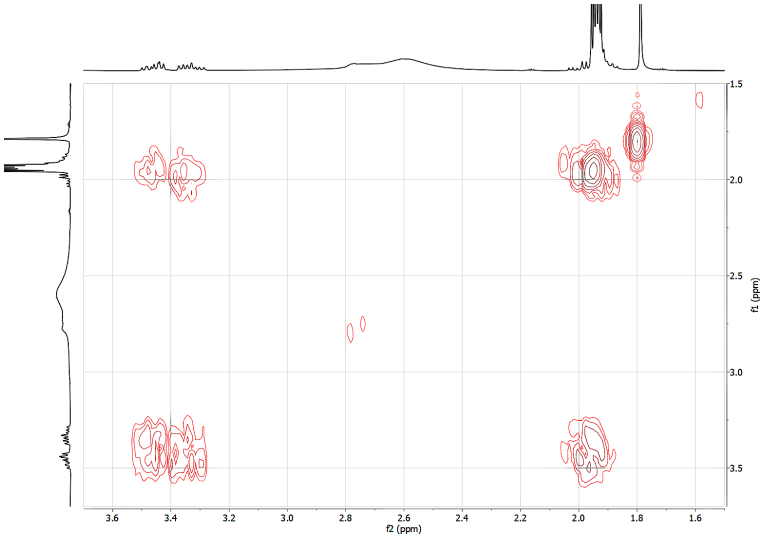

Figure AII.16. $^{1}H-^{1}H$-COSY NMR spectrum of [**2s**]Cl dissolved in CD_3CN. The synthesis was done in absence of triethylamine. The spectrum shows the correlation of protons in N-C**H**$_2$-C**H**$_2$-S (3.18–3.50 ppm) with the solvent peak (1.9 ppm), indicating that the solvent peak obscures the proton peak of interest.

Table AII.1. Crystallographic data for all crystals in the present work.

	[**1s**]Cl	[**2s-Ag-2s**]$(SbF_6)_3$	[**2ssquin**]
Chemical formula	$C_{23}H_{22}CoN_4OS\cdot 3(CH_4O)\cdot Cl$	$C_{50}H_{51}AgCo_2N_9O_2S_2\cdot 3(F_6Sb)\cdot 0.969(C_2H_3N)$	$C_{48}H_{48}Cl_2Co_2N_8O_2S_2\cdot 0.903(C_2H_3N)$
M_r	593.01	1846.88	1058.87
Crystal system	Triclinic	Monoclinic	Monoclinic
Space group	*P*-1	$P2_1/c$	$P2_1/n$
Cell lengths (*a, b, c*) (Å)	8.8184(3), 13.0506(5), 13.3362(5)	15.7072(5), 27.0793(6), 19.3101(6)	18.4673(4), 14.9350(4), 19.1135(4)
Cell angles (α, β, γ) (°)	63.783(4), 73.530(3), 84.488(3)	90, 112.171(3), 90	90, 97.898(2), 90
Cell volume (Å^3)	1319.66(10)	7606.1 (4)	5221.7(2)
Z	2	4	4
μ (mm^{-1})	7.11	1.87	0.86
Crystal size (mm)	0.41 × 0.33 × 0.18	0.52 × 0.37 × 0.22	0.35 × 0.22 × 0.20
Temperature (K)	110(2)	110(2)	110(2)
Diffractometer	SuperNova, Dual, Cu at zero, Atlas detector	SuperNova, Dual, Cu at zero, Atlas detector	SuperNova, Dual, Cu at zero, Atlas detector
Radiation type	Cu *K*α	Mo *K*α	Mo *K*α
T_{min}, T_{max}	0.161, 0.410	0.295, 1.000	0.425, 1.000
No. of measured, independent and observed [$I > 2\sigma(I)$] reflections	16974, 5155, 5078	61799, 21893, 14227	62110, 11982, 9923
R_{int}	0.025	0.048	0.045
$(\sin\theta/\lambda)_{max}$ (Å^{-1})	0.616	0.650	0.650
$R[F^2 > 2\sigma(F^2)]$, $wR(F^2)$, S	0.028, 0.071, 1.05	0.072, 0.231, 1.07	0.048, 0.128, 1.03
No. of reflections	5155	21893	11982
No. of parameters	340	1385	618
No. of restraints	-	2501	2
H-atom treatment	H-atom parameters constrained	H-atom parameters constrained	H-atom parameters constrained
$\Delta\rho_{max}$, $\Delta\rho_{min}$ (e Å^{-3})	0.28, −0.46	1.75, −1.28	0.69, −0.59

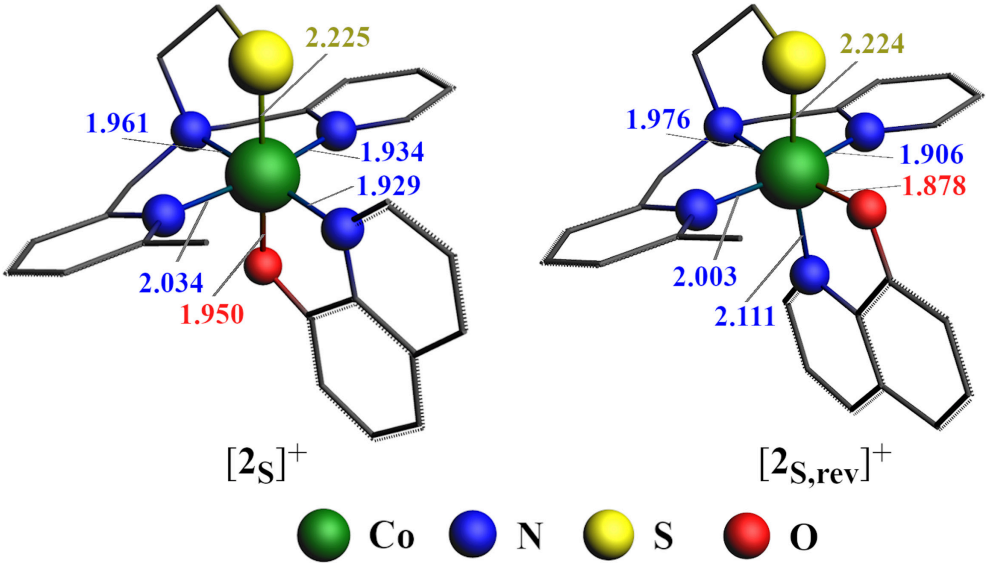

Figure AII.17. Optimized geometries of $[\mathbf{2}_{\mathbf{S}}]^{+}$ and $[\mathbf{2}_{\mathbf{S,rev}}]^{+}$ with selected bond distances (Å).

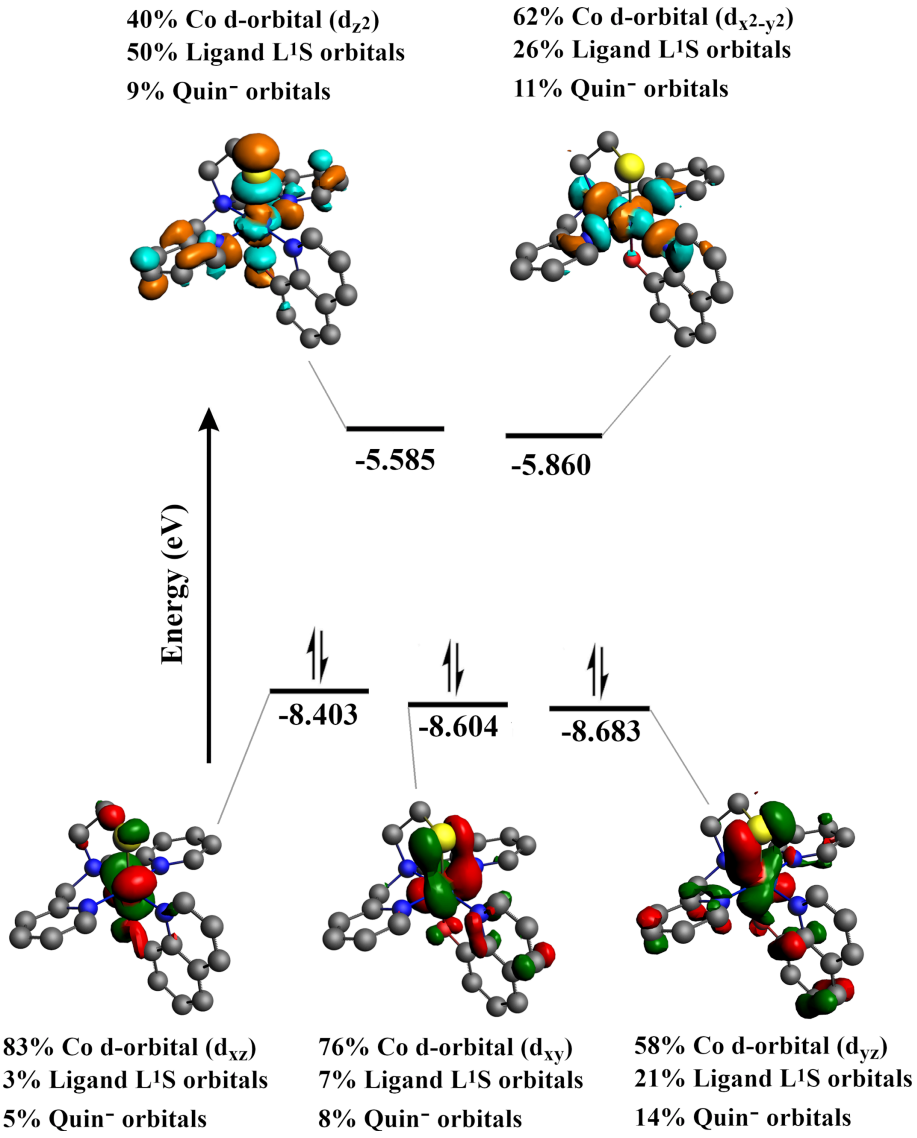

Figure AII.18. Several frontier orbitals of $[\mathbf{1s}]^+$ associated with Co *d*-orbitals along with their energies, orbital visualization, and orbital composition.

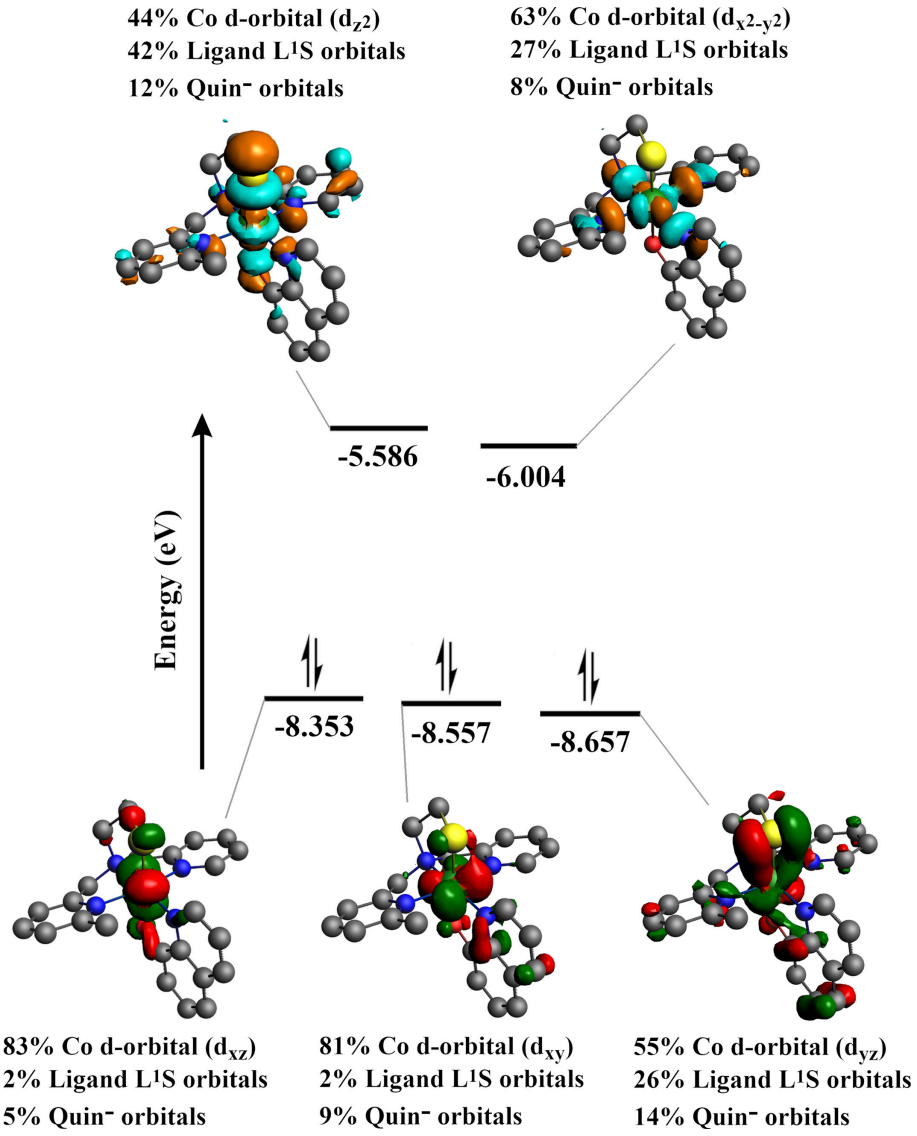

Figure AII.19. Several frontier orbitals of $[\mathbf{2s}]^+$ associated with Co *d*-orbitals along with their energies, orbital visualization, and orbital composition.

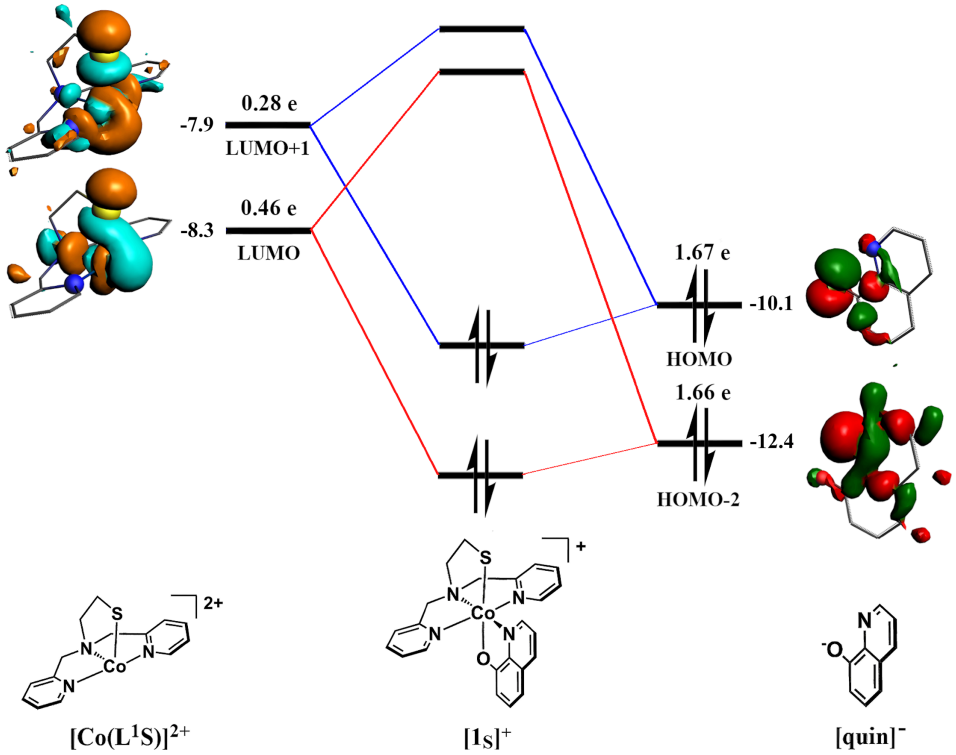

Figure AII.20. Molecular orbital diagram for the interaction between the fragments $[Co(L^1S)]^{2+}$ and $[quin]^-$ in $[\mathbf{1}_S]^+$. Fragment molecular orbital energies (in eV) obtained from the Kohn-Sham Fock matrix diagonal elements (see references [1-3] for details).

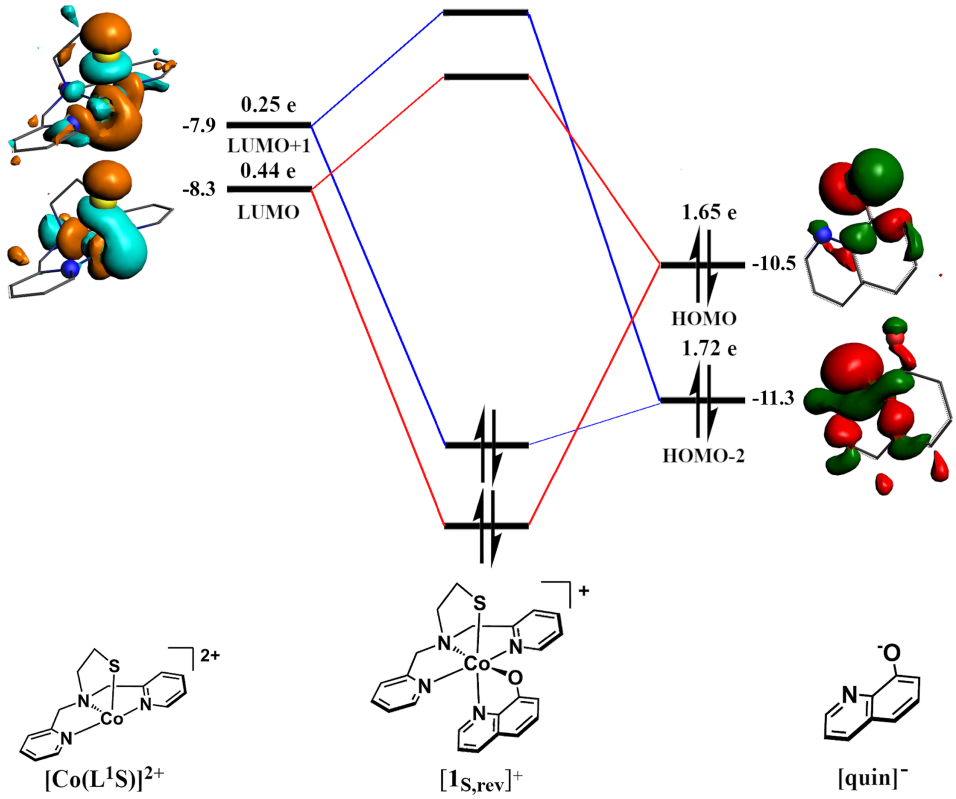

Figure AII.21. Molecular orbital diagram for the interaction between the fragments $[Co(L^1S)]^{2+}$ and $[quin]^-$ in $[\mathbf{1}_{S,rev}]^+$. Fragment molecular orbital energies (in eV) obtained from the Kohn-Sham Fock matrix diagonal elements (see references [1-3] for details).

References

1. Bickelhaupt, F. M., Solà, M. and Fonseca Guerra, C. *J. Mol. Model.* **2006**, 12 (5), 563-568.
2. Bickelhaupt, F. M., Solà, M. and Fonseca Guerra, C. *Inorg. Chem.* **2007**, 46 (13), 5411-5418.
3. Bickelhaupt, F. M., Solà, M. and Guerra, C. F. *J. Comput. Chem.* **2007**, 28 (1), 238-250.

Appendix III

Supplementary Information for Chapter 4

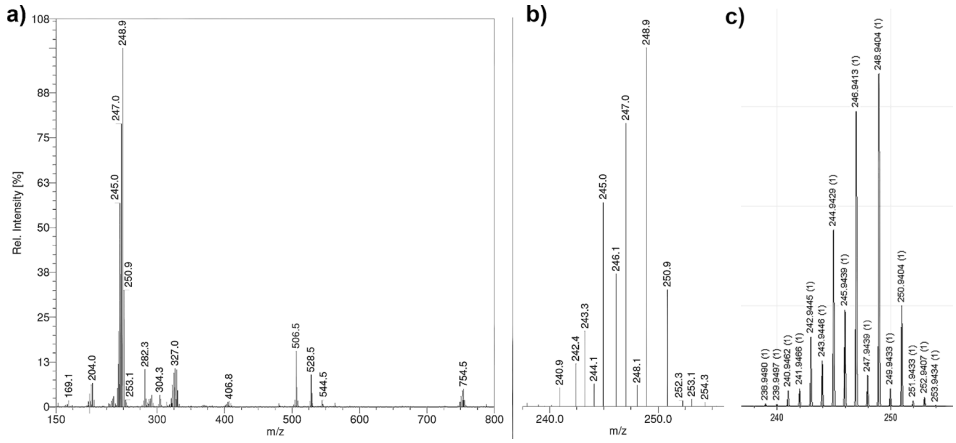

Figure AIII.1. ESI-MS spectrum of a) selenocystamine hydrochloride; b) the experimental isotopic distribution of the main signal; c) simulated isotopic distribution. ESI-MS found (calcd.) for $[(NH_2C_2H_4Se)_2 + H]^+$ *m/z* 248.9 (248.94).

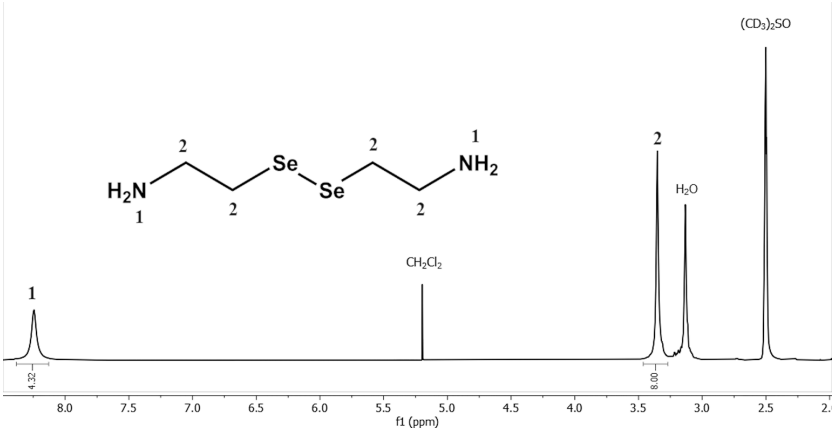

Figure AIII.2. ^{1}H-NMR spectrum of selenocystamine hydrochloride in $(CD_3)_2SO$.

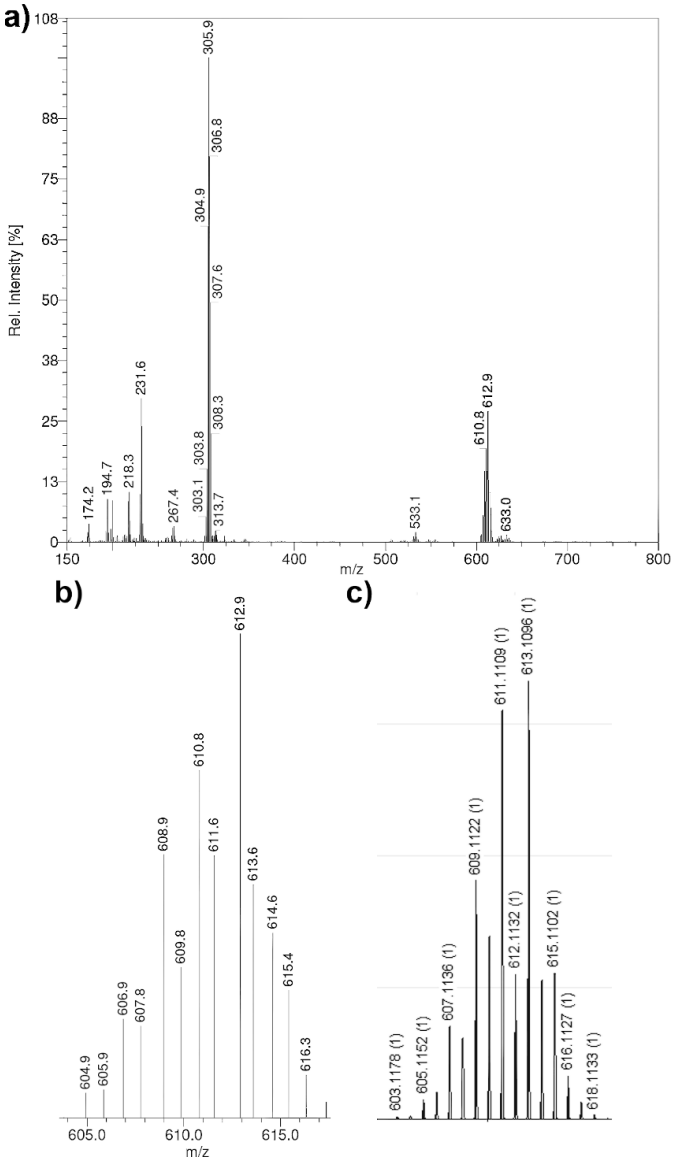

Figure AIII.3. ESI-MS spectrum of a) L^1SeSeL^1; b) the experimental isotopic distribution of the main signal; c) simulated isotopic distribution. ESI-MS found (calcd.) for $[L^1SeSeL^1 + H]^+$ *m/z* 612.9 (613.1) and for $[L^1SeSeL^1 + 2H]^{2+}$ *m/z* 306.8 (307.06).

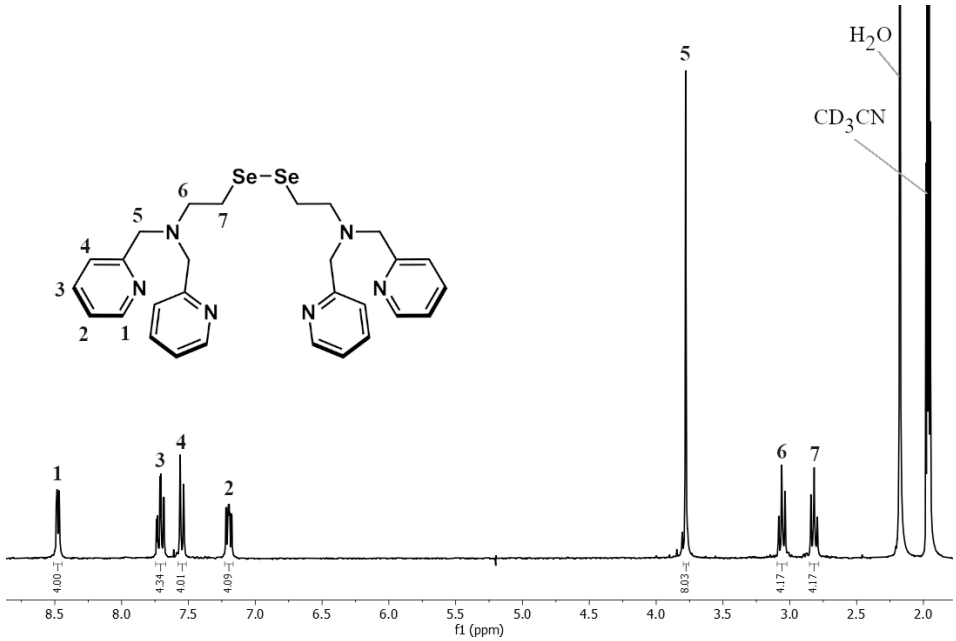

Figure AIII.4. ^{1}H-NMR spectrum of L^{1}SeSeL^{1} in CD_3CN.

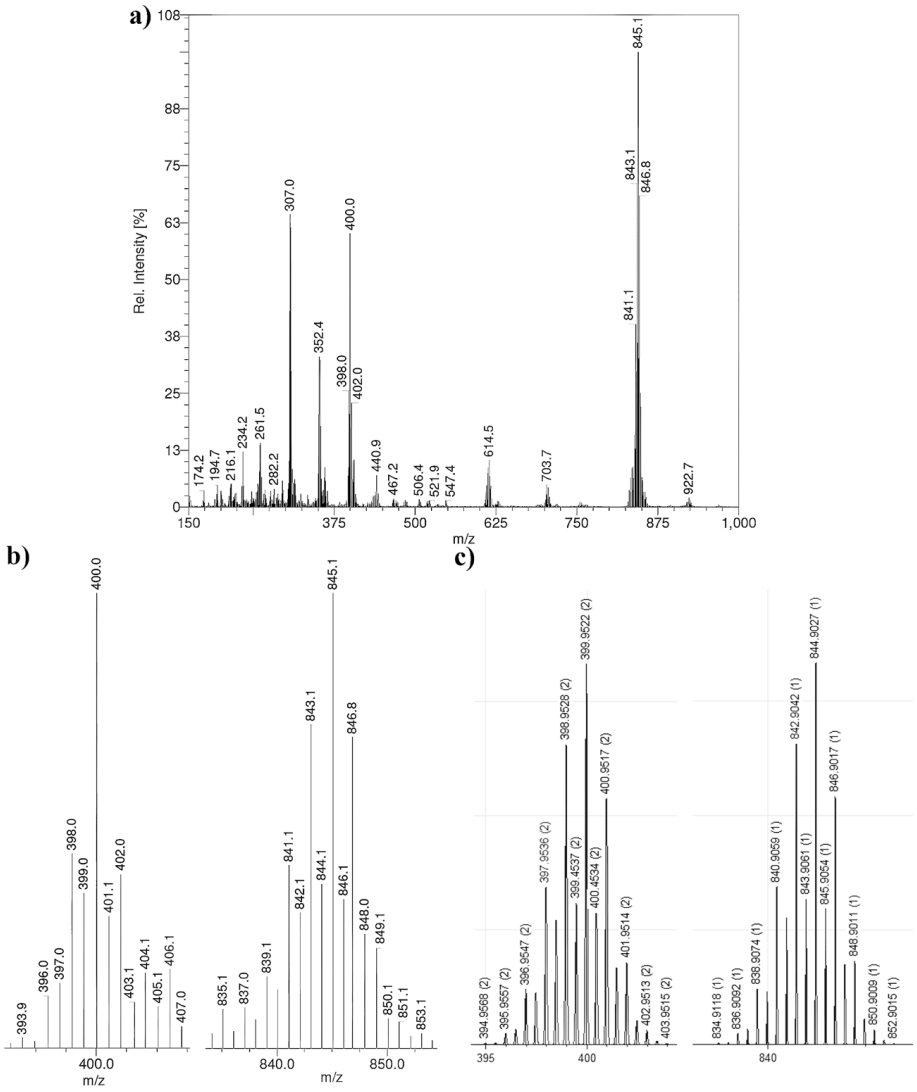

Figure AIII.5. ESI-MS spectrum of a) $[Co_2(L^1SeSeL^1)(Cl)_4]$ ([**1**]); b) the experimental isotopic distribution of the main peaks; c) simulated isotopic distribution. ESI-MS found (calcd.) for $[\mathbf{1} - 2Cl^-]^{2+}$ *m/z* 400.0 (399.95) and for $[\mathbf{1} - 2Cl^- + HCOO^-]^+$ *m/z* 845.1 (844.90).

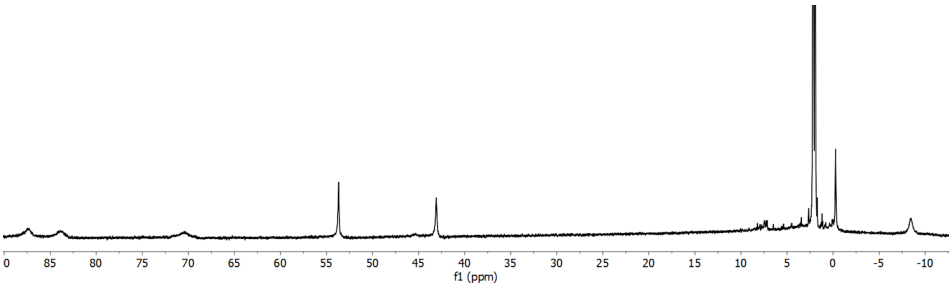

Figure AIII.6. ^{1}H-NMR spectrum of compound [**1**] in CD_3CN.

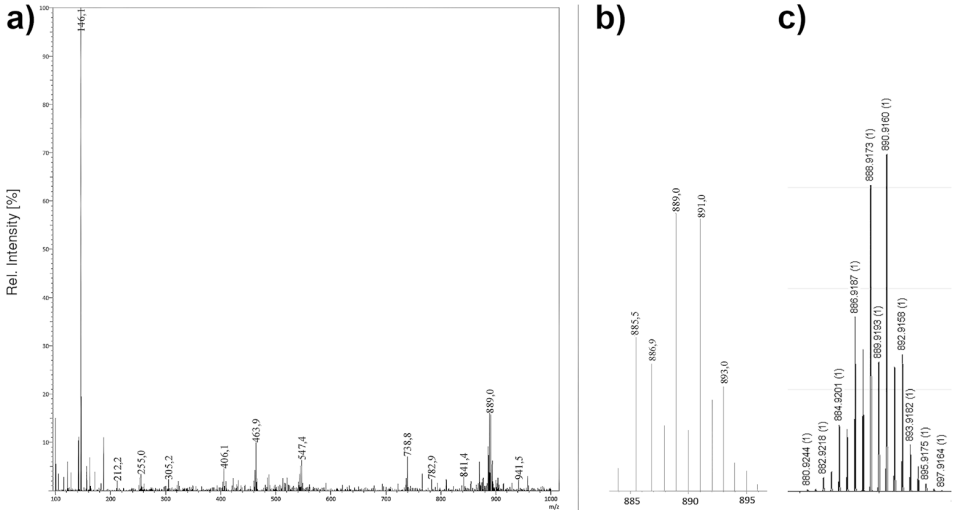

Figure AIII.7. ESI-MS spectrum of a) [Co(L^{1}Se)(NCS)$_2$] ([**2**]); b) the experimental isotopic distribution of the main signal; c) simulated isotopic distribution. ESI-MS found (calcd.) for [**2** – SCN^- + MeCN]$^+$ *m/z* 463.9 (463.99), for [2×**2** – 2SCN^- + $HCOO^-$]$^+$ *m/z* 889.0 (888.92).

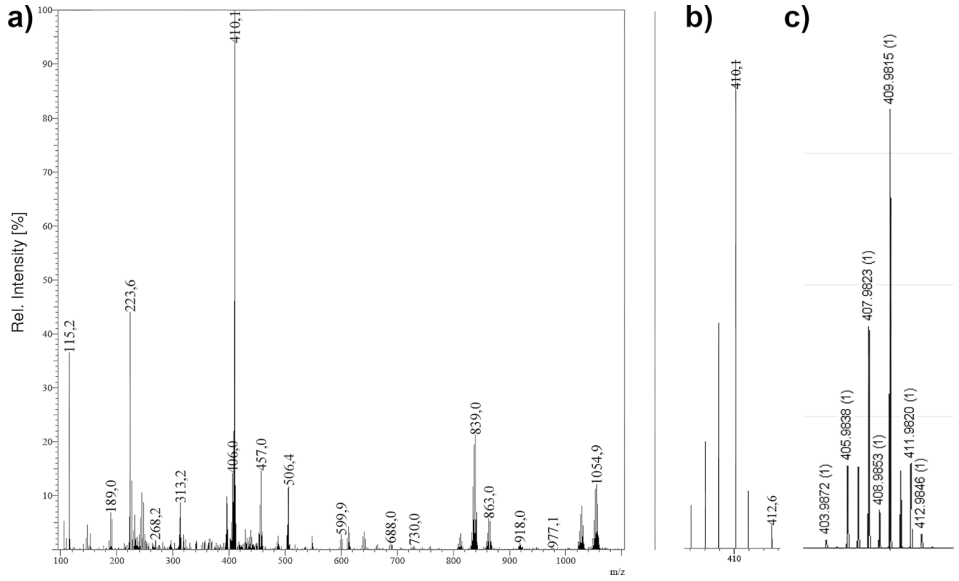

Figure AIII.8. ESI-MS spectrum of a) $[Co(L^1Se)(MeCN)_2](SbF_6)_2$ ([**3**]$(SbF_6)_2$); b) the experimental isotopic distribution of the main signal; c) simulated isotopic distribution. ESI-MS found (calcd.) for $[\mathbf{3}]^{2+}$ *m/z* 223.6 (223.52), for $[\mathbf{3} - 2MeCN + HCOO^-]^+$ *m/z* 410.1 (409.98), for the dimer $[2\times\mathbf{3} - 4MeCN + 3HCOO^-]^+$ *m/z* 863.0 (862.96), and $[2\times\mathbf{3} - 4MeCN + 2HCOO^- + SbF_6^-]^+$ *m/z* 1054.9 (1054.86).

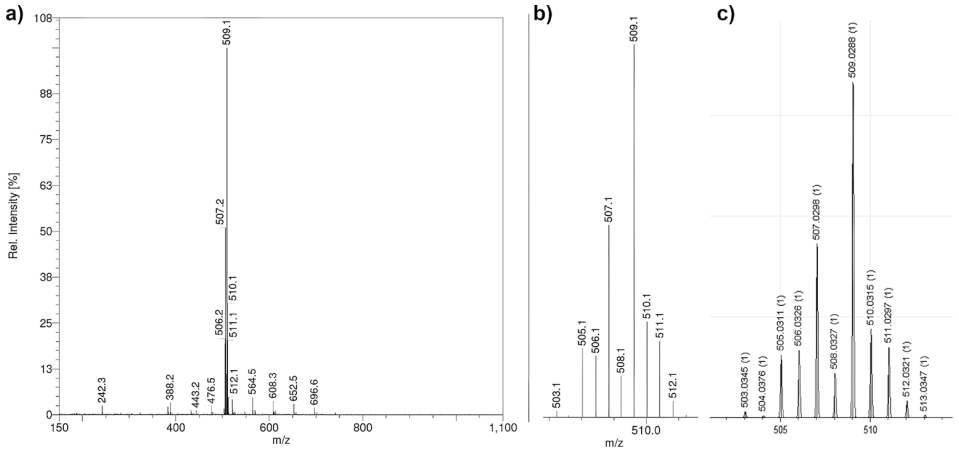

Figure AIII.9. ESI-MS spectrum of a) compound $[Co(L^1Se)(quin)]Cl$ ([**4**]Cl); b) the experimental isotopic distribution of the main signal; c) simulated isotopic distribution. ESI-MS found (calcd.) for $[\mathbf{4}]^+$ *m/z* 509.1 (509.03).

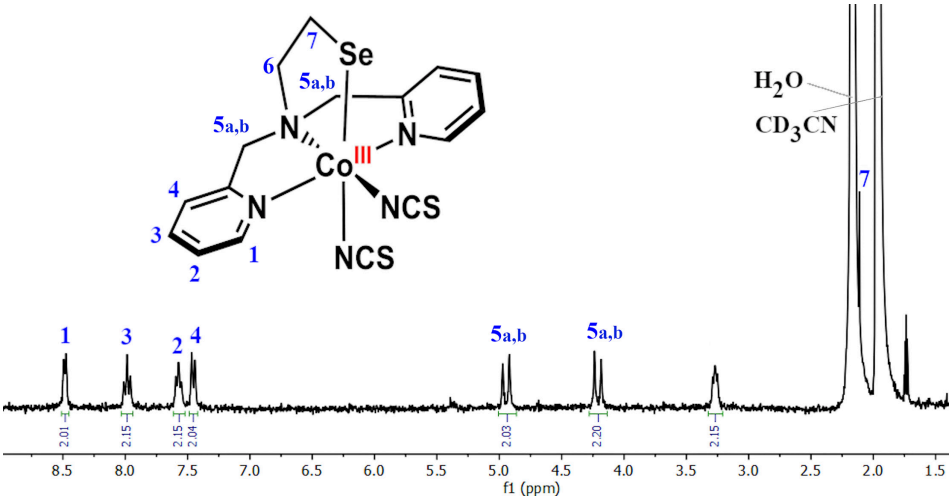

Figure AIII.10. ^{1}H-NMR spectrum of compound [**2**] dissolved in CD_3CN.

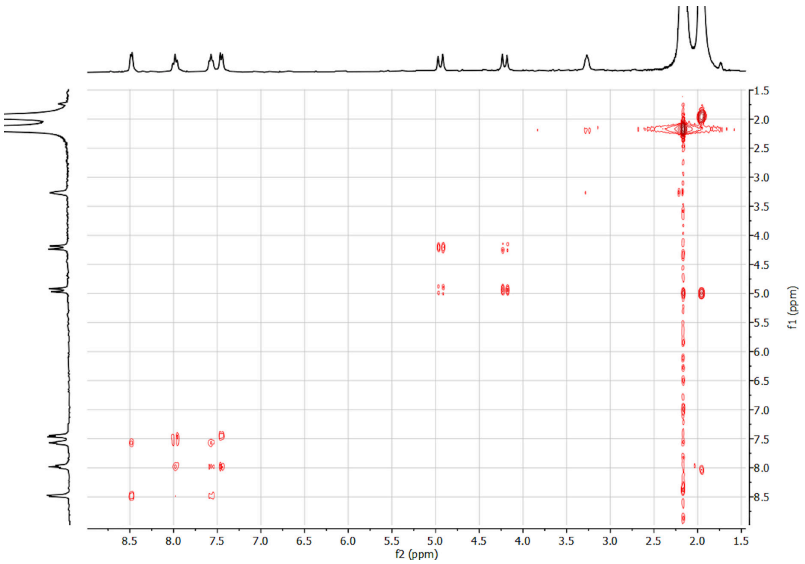

Figure AIII.11. ^{1}H-^{1}H COSY NMR spectrum of compound [**2**] dissolved in CD_3CN.

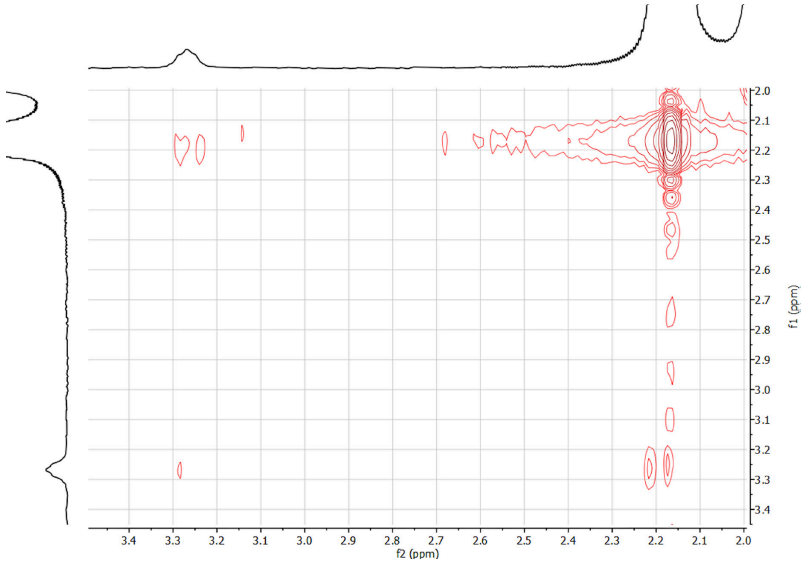

Figure AIII.12. ^{1}H-^{1}H COSY NMR spectrum at 2.0-3.5 ppm of compound [**2**] dissolved in CD_3CN. The correlation of the H_2N-C**H$_2$**-CH_2-Se (about 3.3 ppm) with H_2N-CH_2-C**H$_2$**-Se (about 2.1-2.2 ppm) is shown.

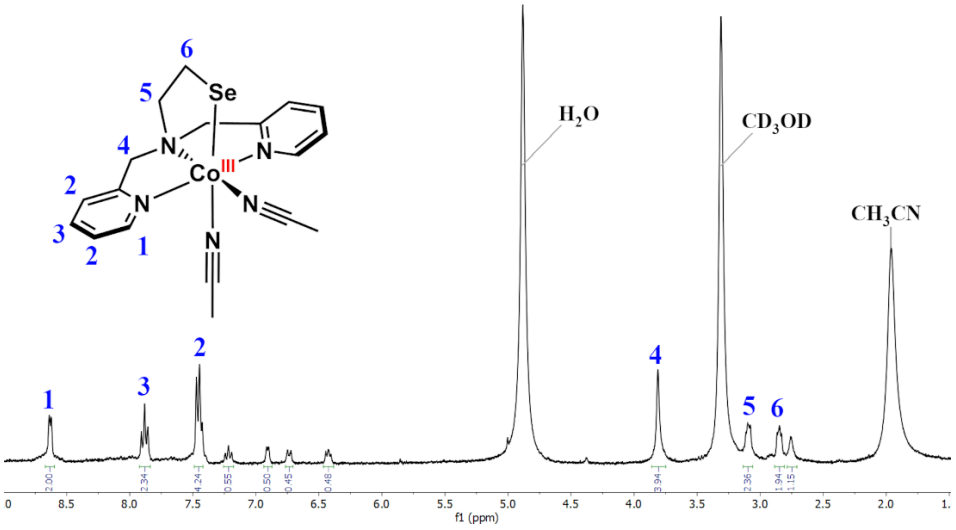

Figure AIII.13. ^{1}H-NMR spectrum [**3**]$(SbF_6)_2$ dissolved in CD_3OD. The spectrum shows unassigned aromatic peaks at 6.4-7.25 ppm and an aliphatic peak at 2.75 ppm, most likely arises from the degradation of the ligand.

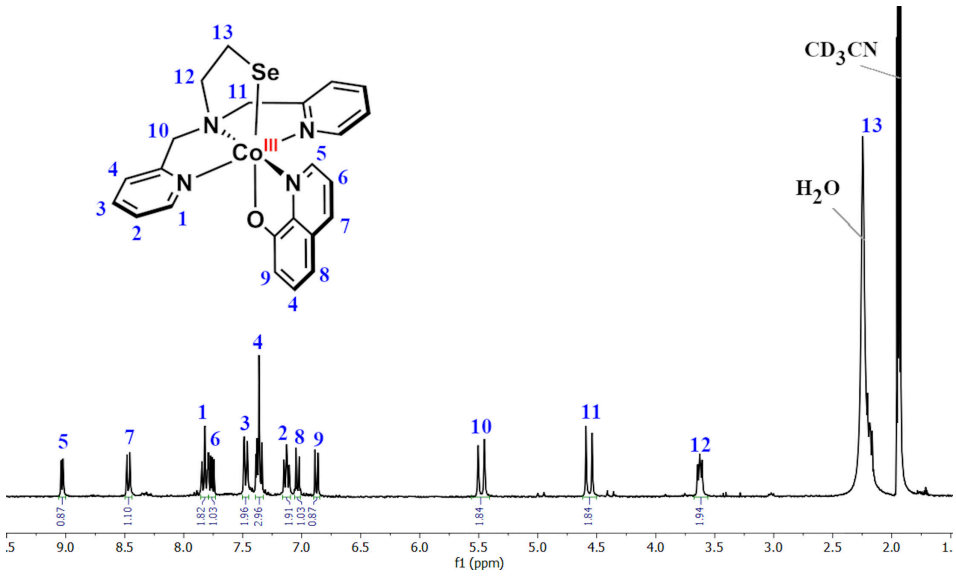

Figure AIII.14. ^{1}H-NMR spectrum of compound [**4**]Cl dissolved in CD_3CN.

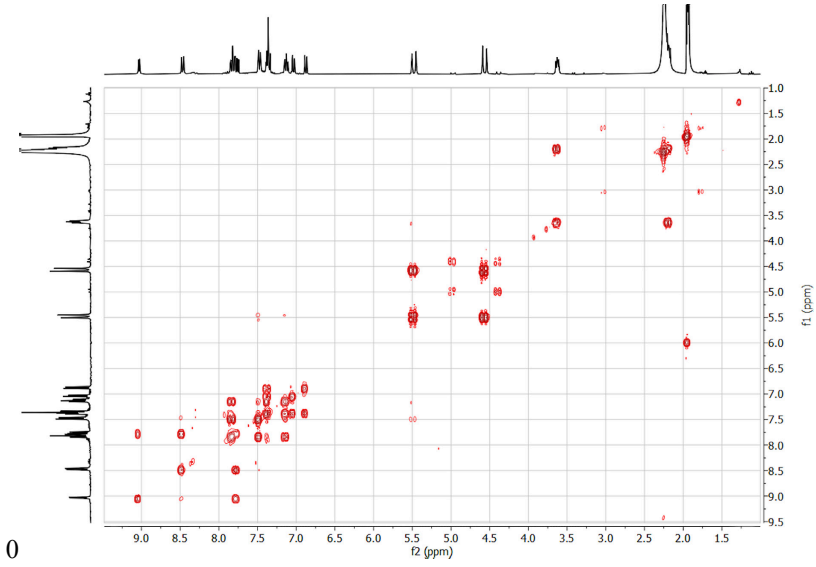

Figure AIII.15. ^{1}H-^{1}H COSY NMR spectrum of compound [**4**]Cl dissolved in CD_3CN.

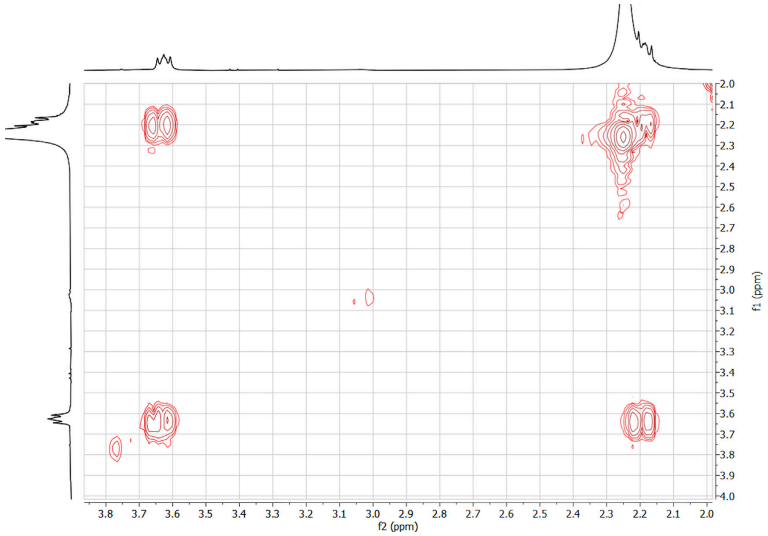

Figure AIII.16. ^{1}H-^{1}H COSY NMR spectrum at 2.0-4.0 ppm of compound [**4**]Cl dissolved in CD_3CN. The correlation of the H_2N-C**H_2**-CH_2-Se (about 3.6 ppm) with H_2N-CH_2-C**H_2**-Se (about 2.2 ppm) is shown.

Table AIII.1. Crystallographic data for all crystals in the present work.

	[**1**]	[**2**]	[**4**]Cl
Chemical formula	$C_{28}H_{32}Cl_4Co_2N_6Se_2 \cdot C_4H_{10}O$	$C_{16}H_{16}CoN_5S_2Se$	$C_{23}H_{22}CoN_4OSe \cdot 2(CHCl_3) \cdot Cl$
M_r	944.29	480.35	782.52
Crystal system	Triclinic	Orthorhombic	Monoclinic
Space group	*P*−1	*Pbca*	$P2_1/n$
Cell lengths (*a, b, c*) (Å)	8.3598(3) 13.7008(6) 17.2414(14)	11.1298(4) 16.5289(5) 19.6469(7)	13.5307(3) 13.2033(3) 17.4772(4)
Cell angles (α, β, γ) (°)	91.225(5) 101.881(4) 92.102(3)	90 90 90	90 105.487(3) 90
Cell volume (Å^3)	1930.31(19)	3614.3(2)	3008.93(13)
Z	2	8	4
μ (mm^{-1})	3.06	3.20	2.43
Crystal size (mm)	0.22 × 0.13 × 0.03	0.21 × 0.14 × 0.06	0.26 × 0.22 × 0.04
Temperature (K)	110	110	110
Diffractometer	SuperNova, Dual, Cu at zero, Atlas detector	SuperNova, Dual, Cu at zero, Atlas detector	SuperNova, Dual, Cu at zero, Atlas detector
Radiation type	Mo *K*α	Mo *K*α	Mo *K*α
T_{min}, T_{max}	0.470, 1.000	0.552, 1.000	0.467, 1.000
No. of measured, independent and observed [$I > 2\sigma(I)$] reflections	25557, 7594, 5429	32659, 4155, 3485	39269, 6915, 5863
R_{int}	0.071	0.049	0.048
$(\sin\theta/\lambda)_{max}$ (Å^{-1})	0.617	0.650	0.650
$R[F^2 > 2\sigma(F^2)]$, $wR(F^2)$, S	0.048, 0.105, 1.04	0.026, 0.058, 1.06	0.030, 0.068, 1.03
No. of reflections	7594	4155	6915
No. of parameters	426	226	443
No. of restraints	-	-	289
H-atom treatment	H-atom parameters constrained	H-atom parameters constrained	H-atom parameters constrained
$\Delta\rho_{max}$, $\Delta\rho_{min}$ (e Å^{-3})	0.88, −0.55	0.59, −0.37	0.94, −0.81

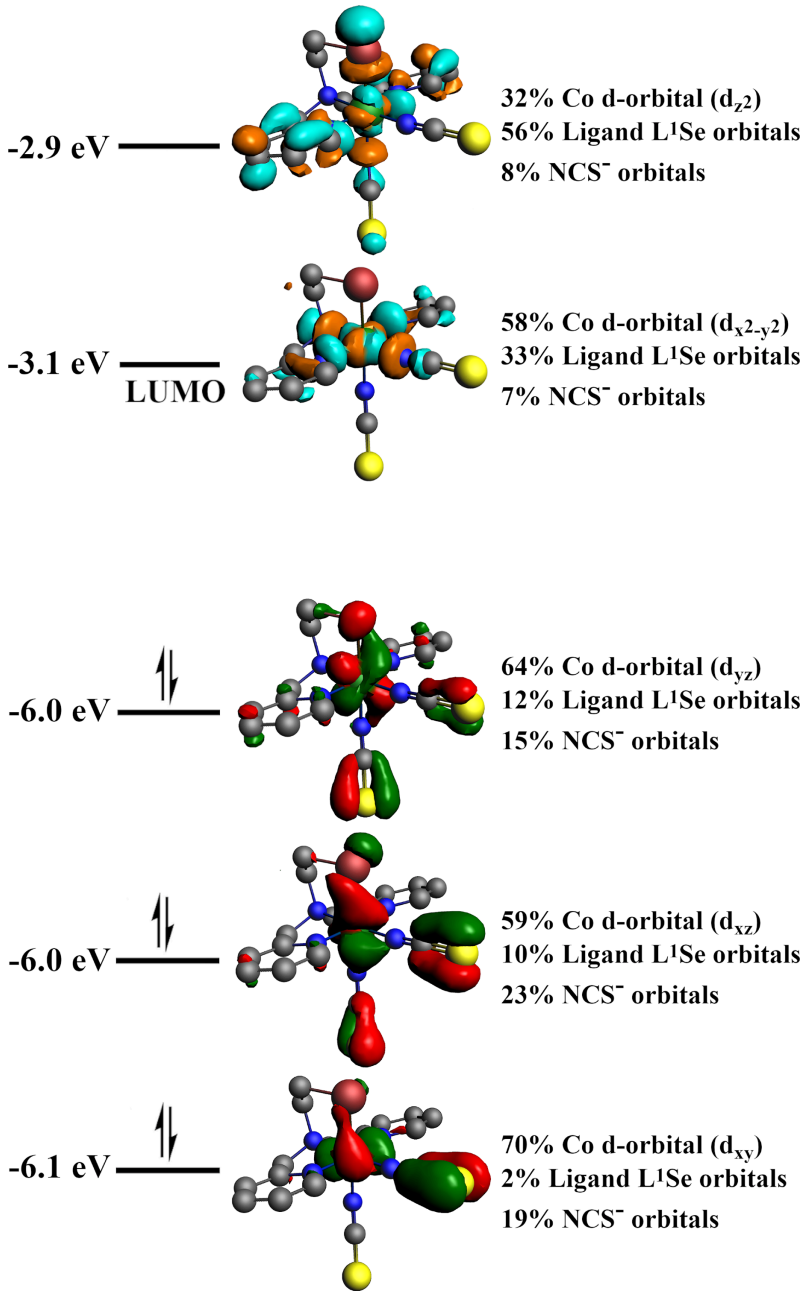

Figure AIII.17. Several frontier orbitals of [**2**] associated with Co *d*-orbitals along with their energies, orbital visualization, and orbital composition.

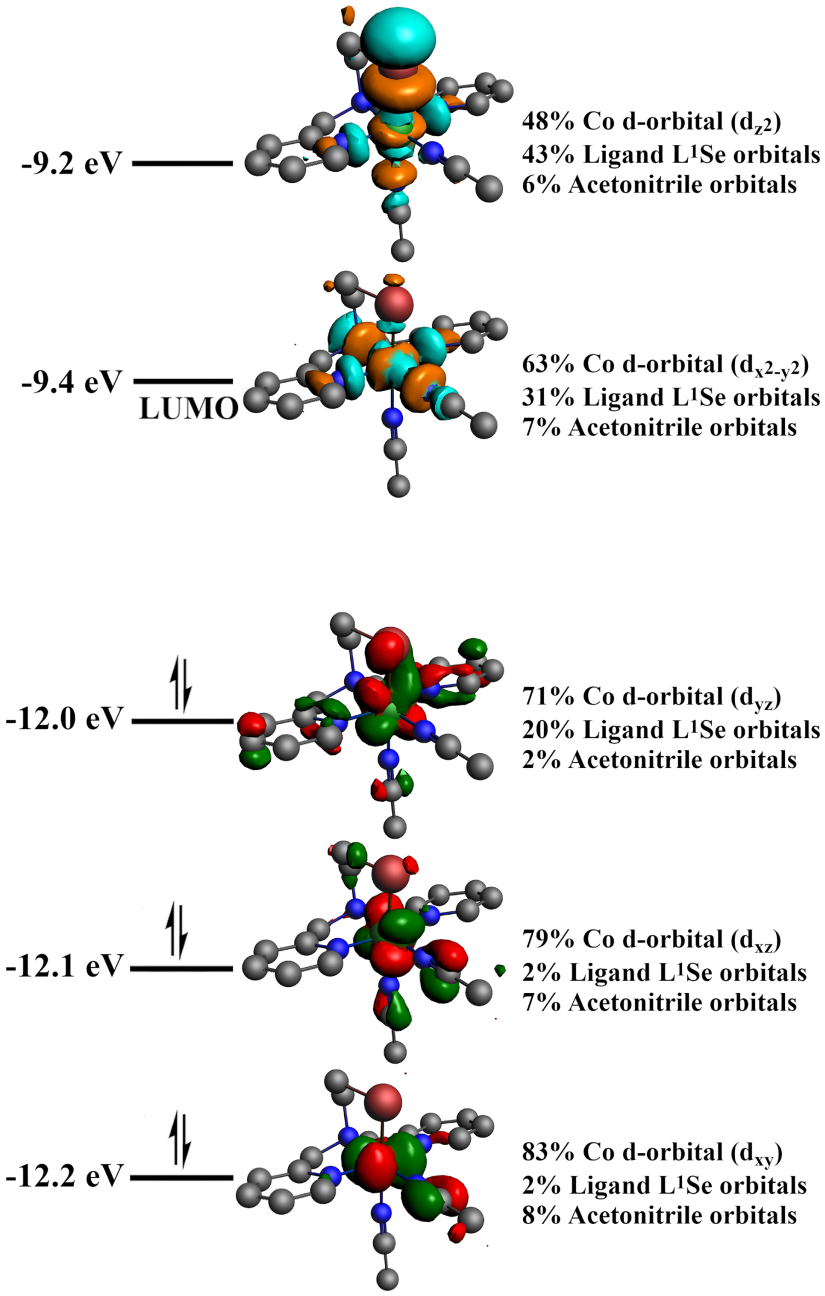

Figure AIII.18. Several frontier orbitals of $[\mathbf{3}]^{2+}$ associated with Co *d*-orbitals along with their energies, orbital visualization, and orbital composition.

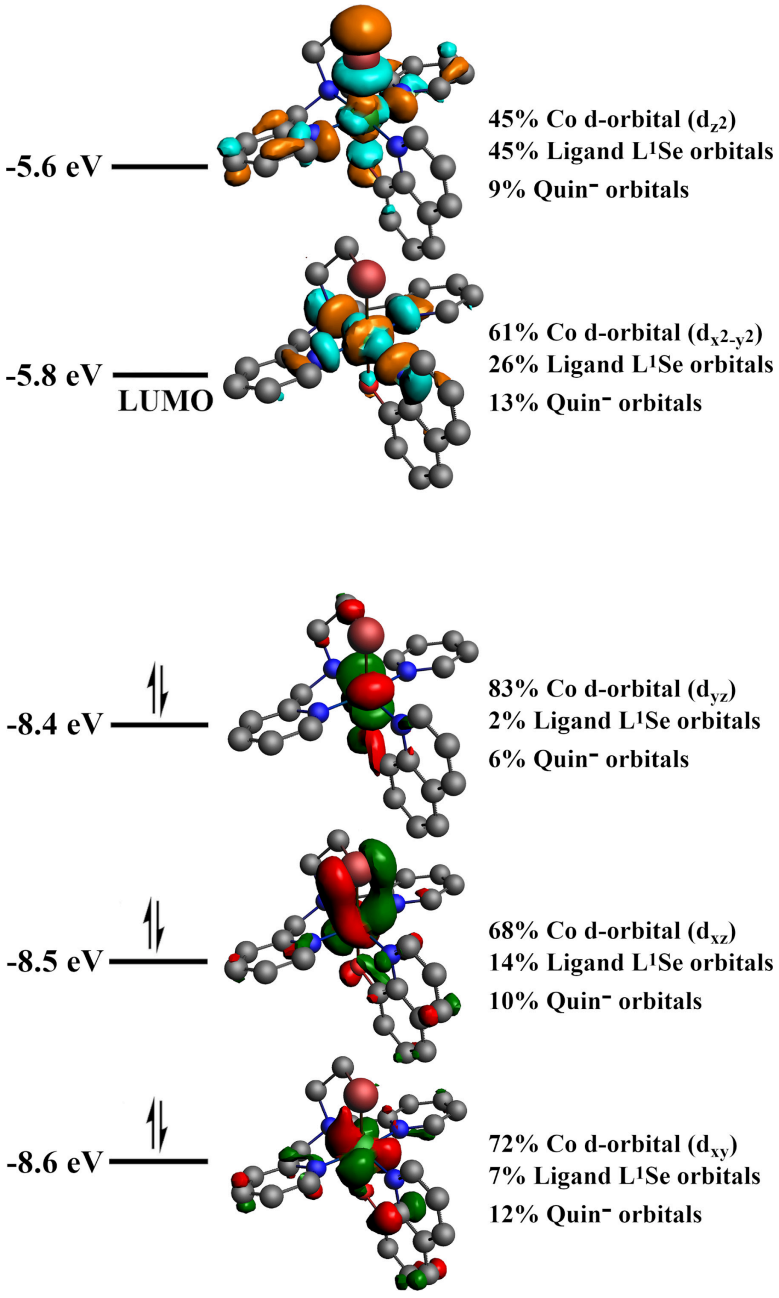

Figure AIII.19. Several frontier orbitals of $[\mathbf{4}]^+$ associated with Co *d*-orbitals along with their energies, orbital visualization, and orbital composition.

Appendix IV

Supplementary Information for Chapter 5

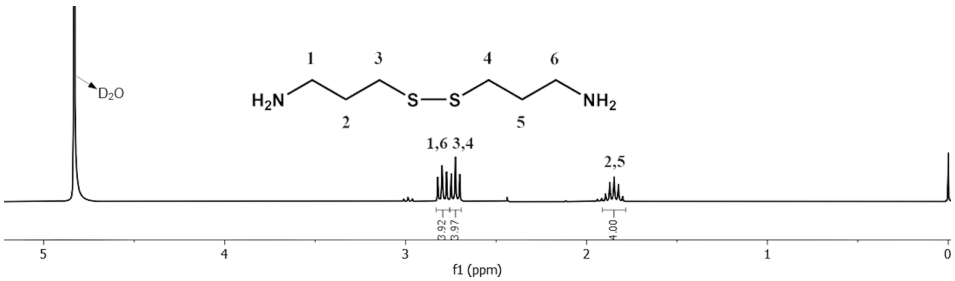

Figure AIV.1. ^{1}H-NMR spectrum of bis(3-aminopropyldisulfide) in D_2O.

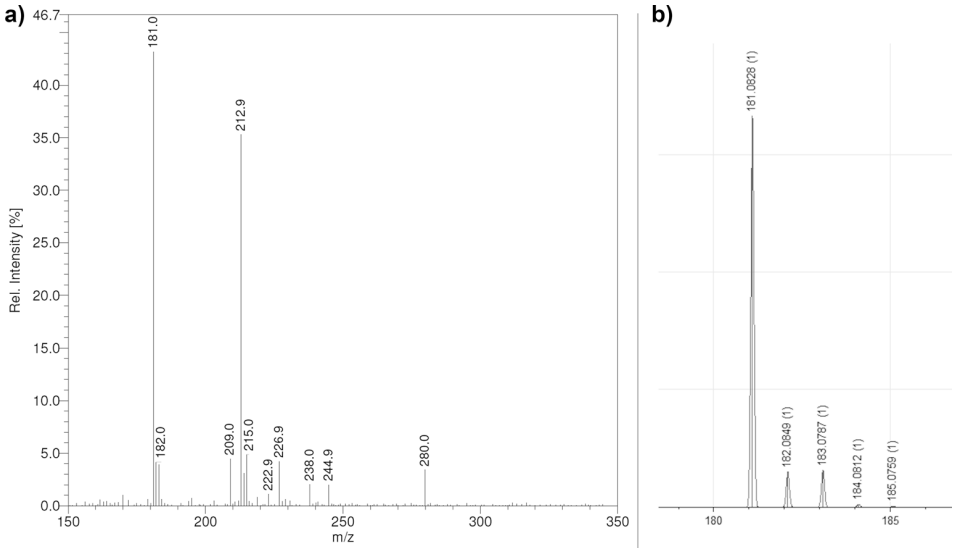

Figure AIV.2. ESI−MS spectrum of a) bis(3-aminopropyldisulfide) dissolved in H_2O; b) simulated spectrum at *m/z* 180−185. ESI−MS found (calcd.) for [bis(3-aminopropyldisulfide) + H]$^{+}$ *m/z* 181.0 (181.08).

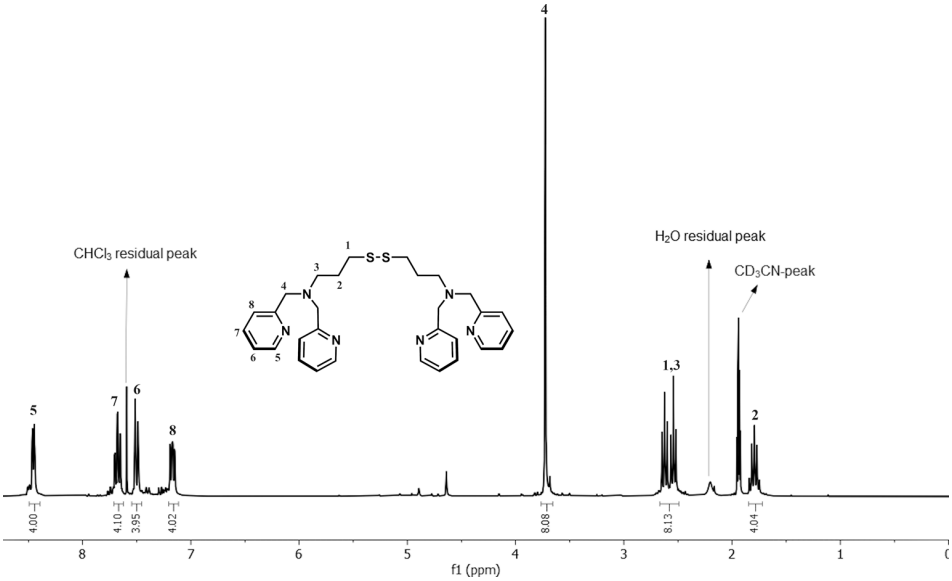

Figure AIV.3. ^{1}H-NMR spectrum of L^{P}SSL^{P} in CD_3CN.

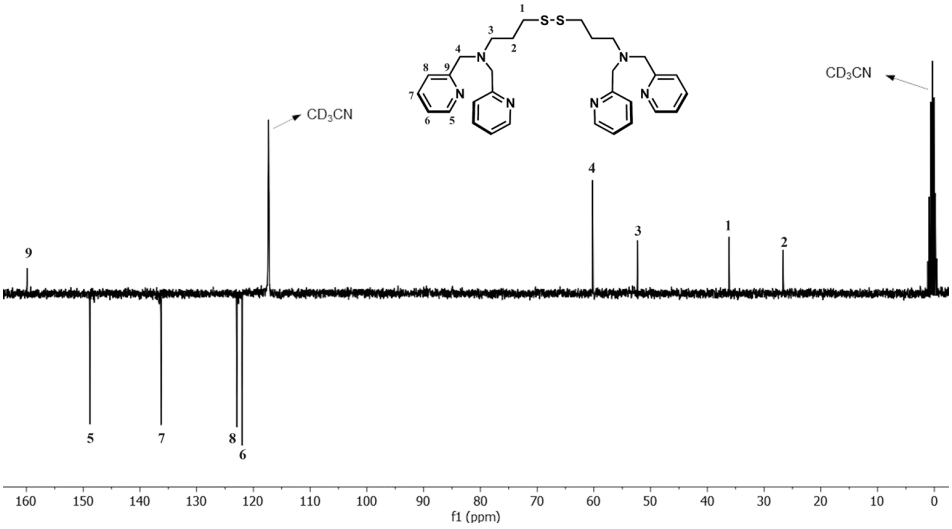

Figure AIV.4. ^{13}C-NMR spectrum of L^{P}SSL^{P} in CD_3CN.

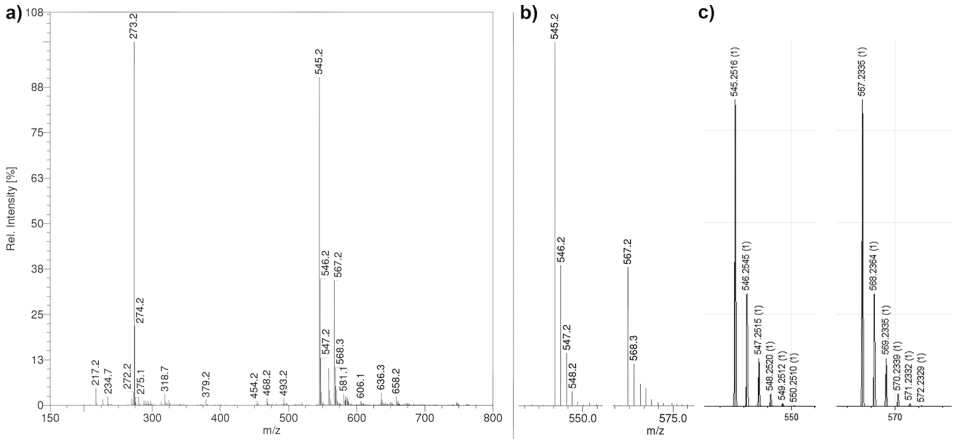

Figure AIV.5. ESI−MS spectrum of a) L^{p}SSL^{p} dissolved in methanol; b) the experimental isotopic distribution; c) simulated isotopic distribution at *m/z* 540−575. ESI−MS found (calcd.) for [L^{p}SSL^{p} + Na]$^{+}$ *m/z* 567.2 (567.2), for [L^{p}SSL^{p} + H]$^{+}$ *m/z* 545.2 (545.2), for [L^{p}SSL^{p} + 2H]$^{2+}$ *m/z* 273.2 (273.1).

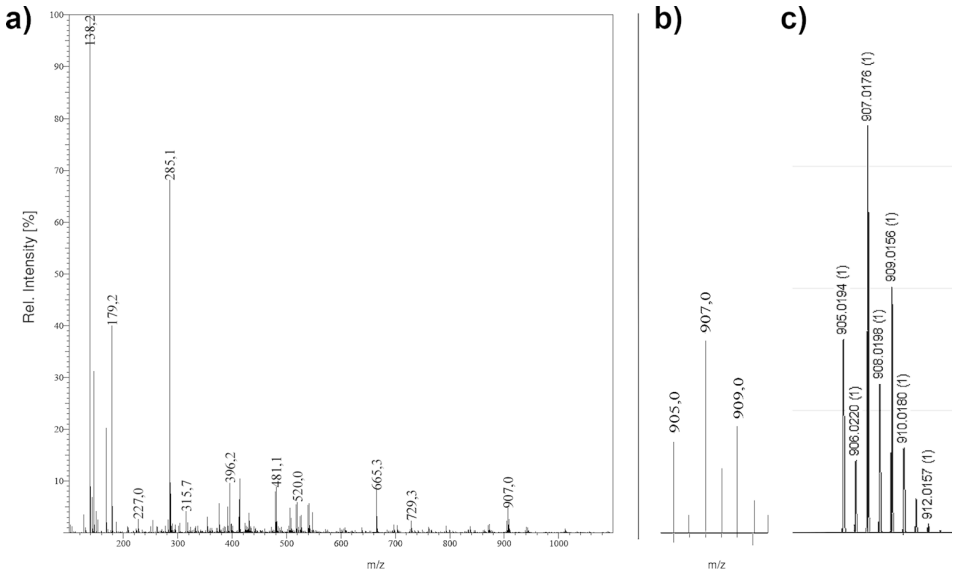

Figure AIV.6. ESI−MS spectrum of a) [$\mathbf{1}_{\mathbf{Br}}$] dissolved in acetonitrile; b) the experimental isotopic distribution; c) simulated isotopic distribution. ESI−MS found (calcd.) for [$\mathbf{1}_{\mathbf{Br}}$ – 2Br^{-} + HCOO^{-}]$^{+}$ *m/z* 907.0 (907.02) and for [$\mathbf{1}_{\mathbf{Br}}$ – 3Br^{-} + HCOO^{-}]$^{2+}$ *m/z* 414.1 (413.5).

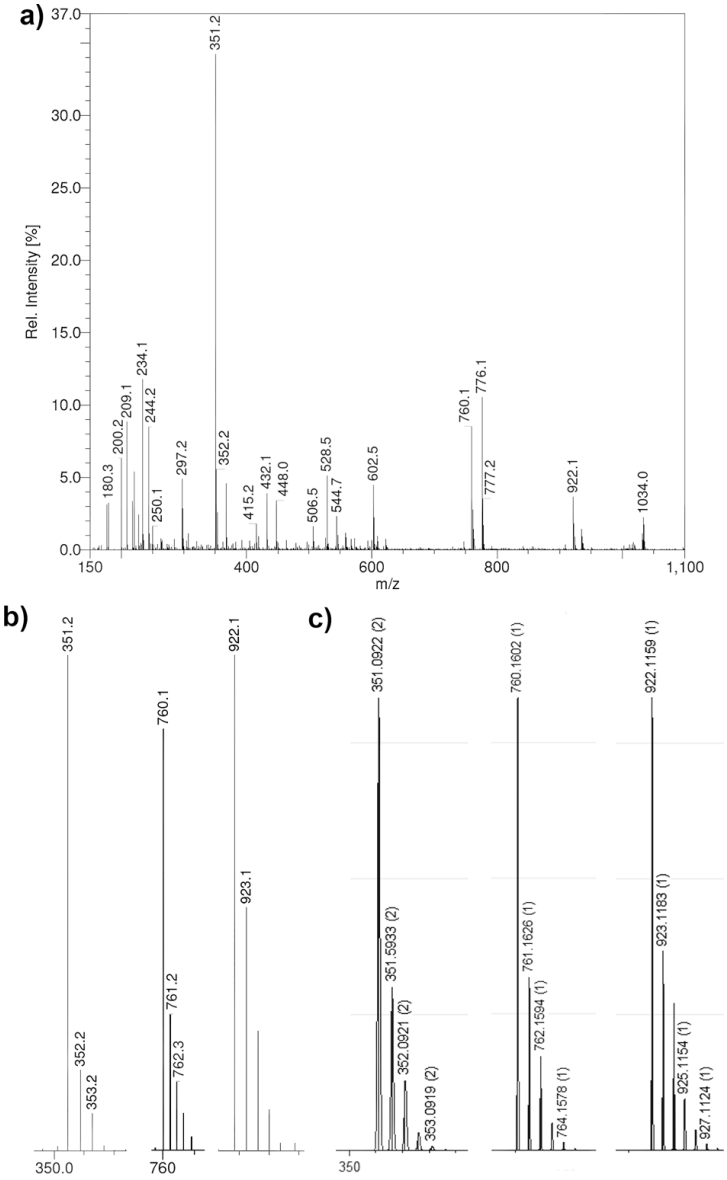

Figure AIV.7. ESI−MS spectrum of a) [$\mathbf{1}_{\mathbf{NCS}}$] dissolved in methanol; b) the experimental isotopic distributions; c) simulated isotopic distributions at different *m/z*. ESI−MS found (calcd.) for [$\mathbf{1}_{\mathbf{NCS}}$ – NCS^- + $HCOO^-$ + H^+]$^+$ *m/z* 922.1 (922.1), for [$\mathbf{1}_{\mathbf{NCS}}$ – $3NCS^-$]$^+$ (partial reduction from the ESI-MS) *m/z* 760.1 (760.16), and for [$\mathbf{1}_{\mathbf{NCS}}$ – $4NCS^-$]$^{2+}$ (partial reduction from the ESI-MS) *m/z* 351.09 (351.1).

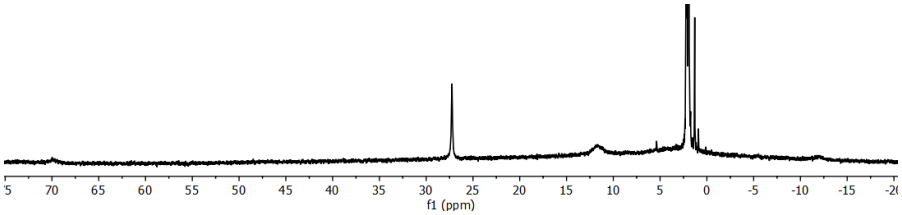

Figure AIV.8. ^{1}H-NMR spectrum of [$\mathbf{1}_{\mathbf{NCS}}$] dissolved in CD_3CN.

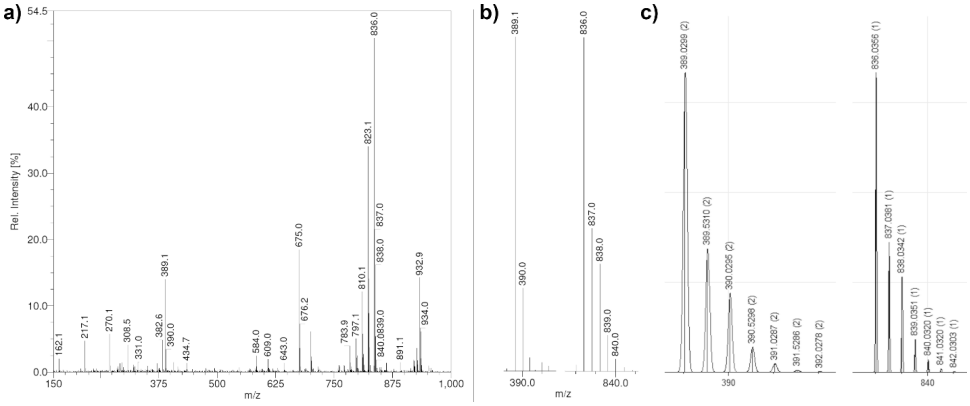

Figure AIV.9. ESI−MS spectrum of a) [$\mathbf{2}_{\mathbf{NCS}}$] dissolved in acetonitrile; b) the experimental isotopic distribution of the main signals; c) simulated isotopic distribution of the main signals. ESI−MS found (calcd.) for [$\mathbf{2}_{\mathbf{NCS}}$ – NCS^-]$^+$ *m/z* 836.0 (836.0), for [$\mathbf{2}_{\mathbf{NCS}}$ – $2NCS^-$]$^{2+}$ *m/z* 389.1 (389.0).

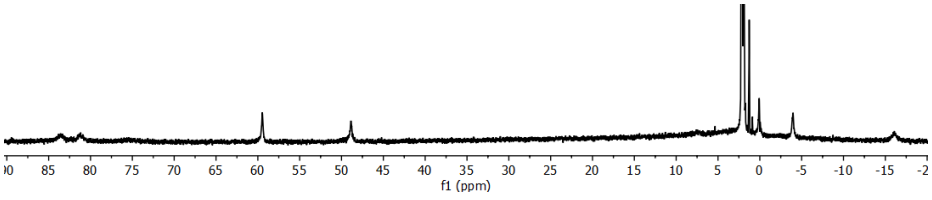

Figure AIV.10. ^{1}H-NMR spectrum of [$\mathbf{2}_{\mathbf{NCS}}$] dissolved in CD_3CN.

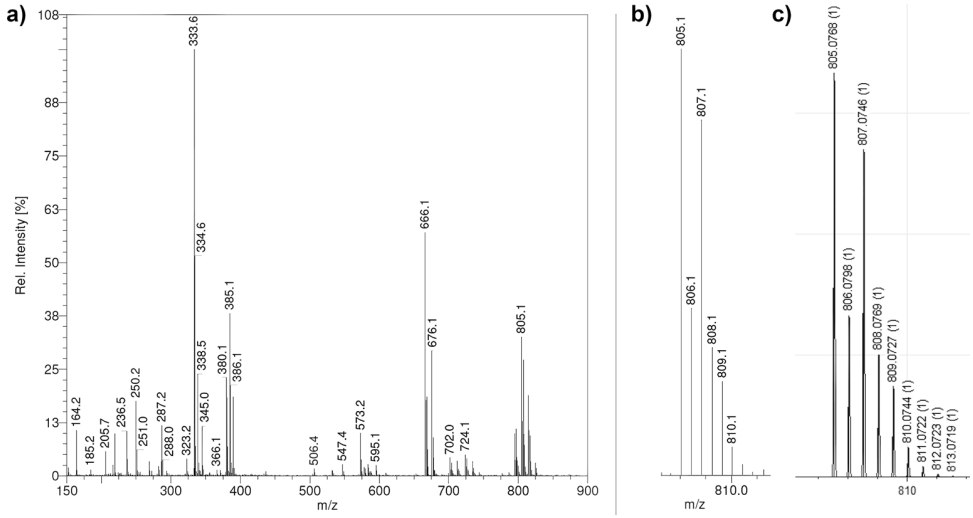

Figure AIV.11. ESI−MS spectrum of compound a) [$\mathbf{3_{Cl}}$] dissolved in methanol; b) the experimental isotopic distribution; c) simulated isotopic distribution at *m/z* 800−815. ESI−MS found (calcd.) for [$\mathbf{3_{Cl}}$ – $2Cl^-$ + $HCOO^-$]$^+$ *m/z* 805.1 (805.08), for [$\mathbf{3_{Cl}}$ – $3Cl^-$ + $HCOO^-$]$^{2+}$ *m/z* 385.1 (385.1), and for [$\mathbf{3_{Cl}}$ – $2Cl^-$]$^{2+}$ *m/z* 380.1 (380.04).

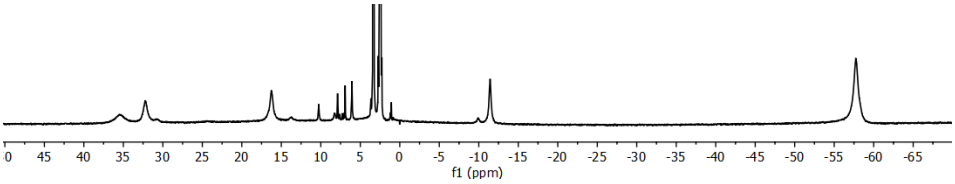

Figure AIV.12. ^{1}H-NMR spectrum of compound [$\mathbf{3_{Cl}}$] dissolved in $(CD_3)_2SO$.

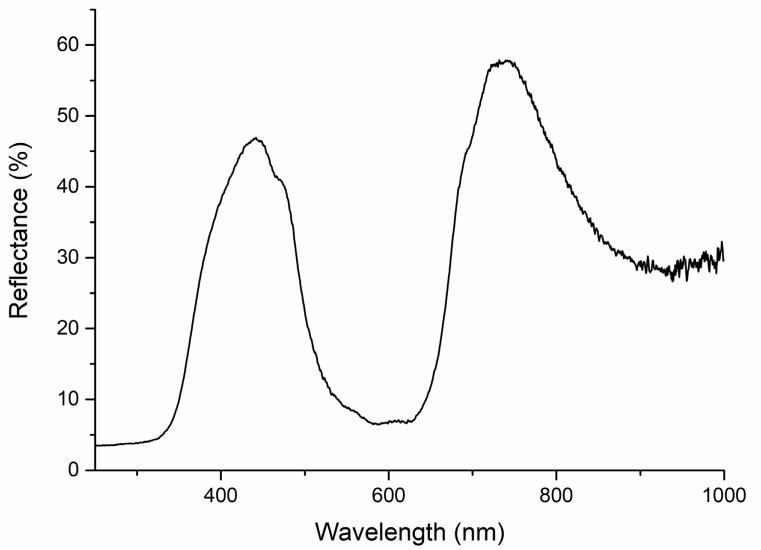

Figure AIV.13. Solid state reflectance spectrum of compound [$\mathbf{1}_{\mathbf{Br}}$].

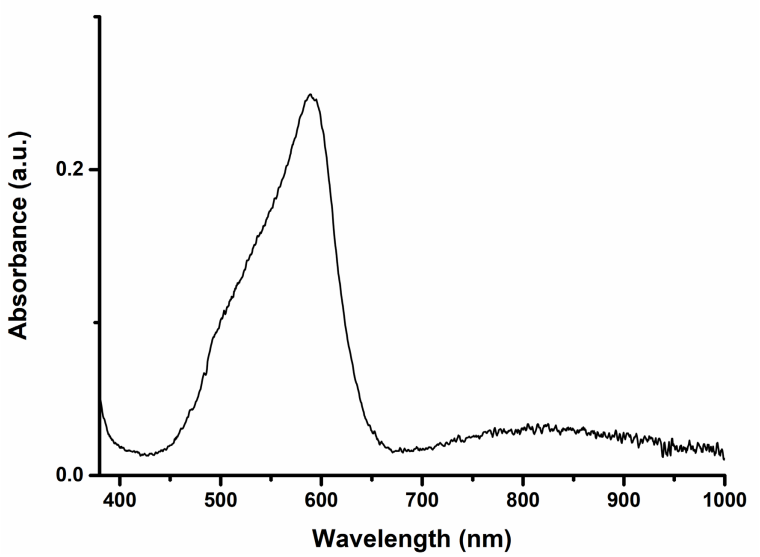

Figure AIV.14. UV-Visible spectrum of 2.5 mM solution of [$\mathbf{1}_{\mathbf{NCS}}$] in acetone, recorded using a transmission dip probe with path length of 1.4 mm.

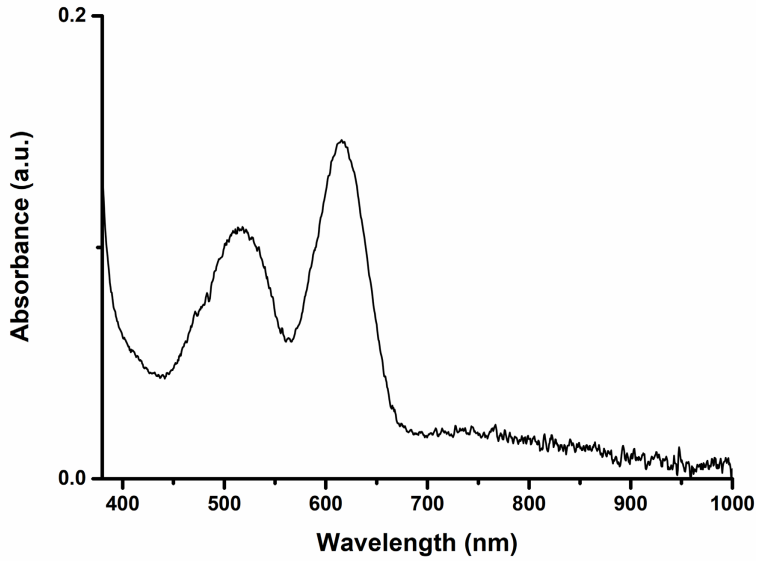

Figure AIV.15. UV-Visible spectrum of 2.5 mM solution of [$\mathbf{2}_{\mathbf{NCS}}$] in acetone, recorded using a transmission dip probe with path length of 1.4 mm.

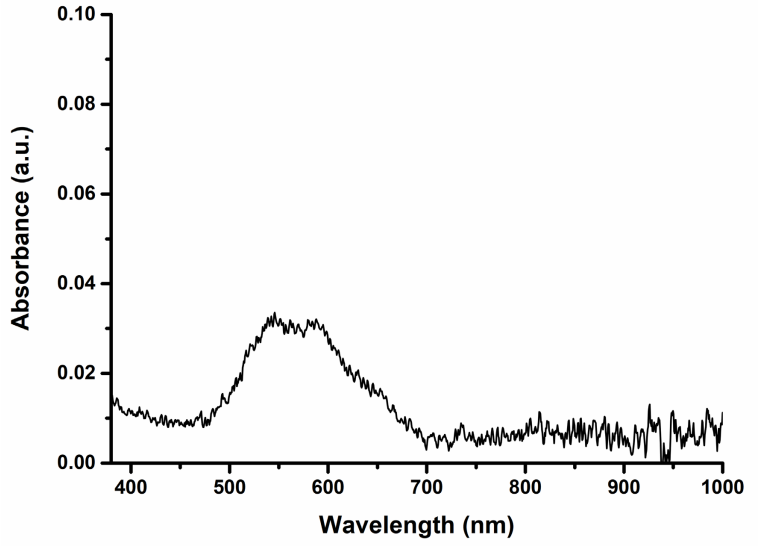

Figure AIV.16. UV-Visible spectrum of 2.5 mM solution of [$\mathbf{3}_{\mathbf{Cl}}$] in acetonitrile, recorded using a transmission dip probe with path length of 1.4 mm.

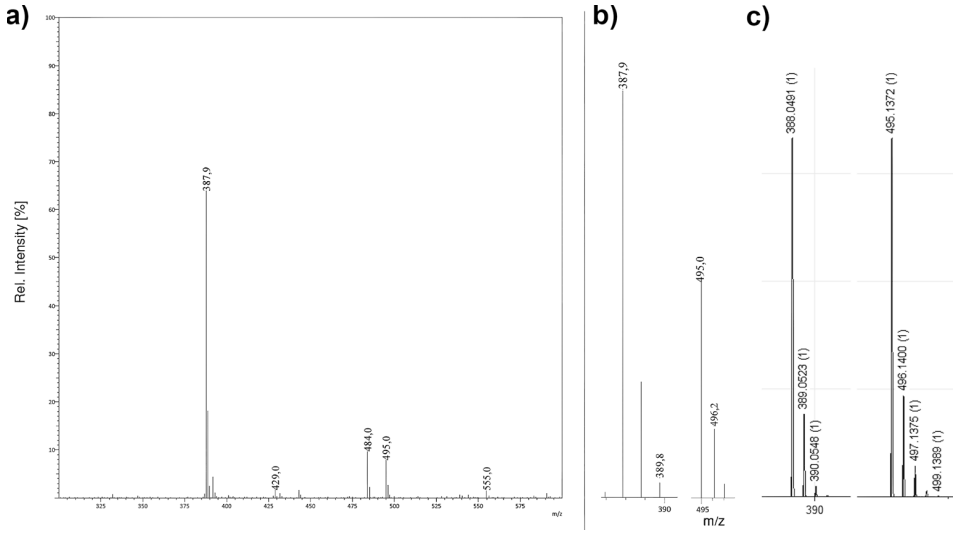

Figure AIV.17. ESI−MS spectrum of a) the reaction of Hquin, K_2CO_3, and *in situ* formed $[Co_2(L^{mpz}SSL^{mpz})(Br)_4]$ dissolved in acetonitrile; b) the experimental isotopic distribution; c) simulated isotopic distribution. ESI−MS found (calcd.) for $[Co(L^{mpz}S)(quin)]^+$ *m/z* 495.0 (495.1), for $[Co(quin)_2(MeCN)]^+$ *m/z* 387.9 (388.0).

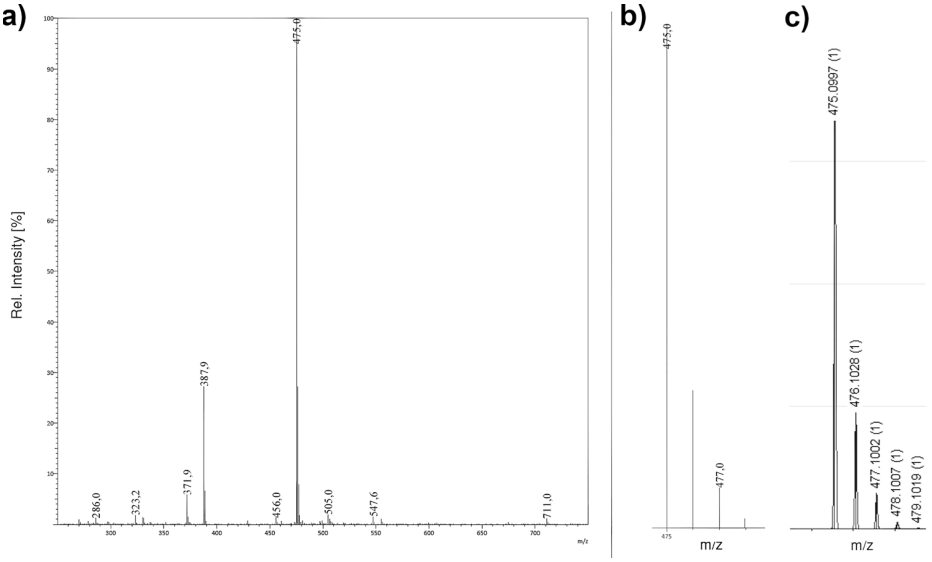

Figure AIV.18. ESI−MS spectrum of a) the reaction of Hquin, K_2CO_3, and *in situ* formed $[Co_2(L^PSSL^P)(Cl)_4]$ dissolved in acetonitrile; b) the experimental isotopic distribution; c) simulated isotopic distribution. ESI−MS found (calcd.) for $[Co(L^PS)(quin)]^+$ *m/z* 475.0 (475.1), for $[Co(quin)_2(MeCN)]^+$ *m/z* 387.9 (388.0).

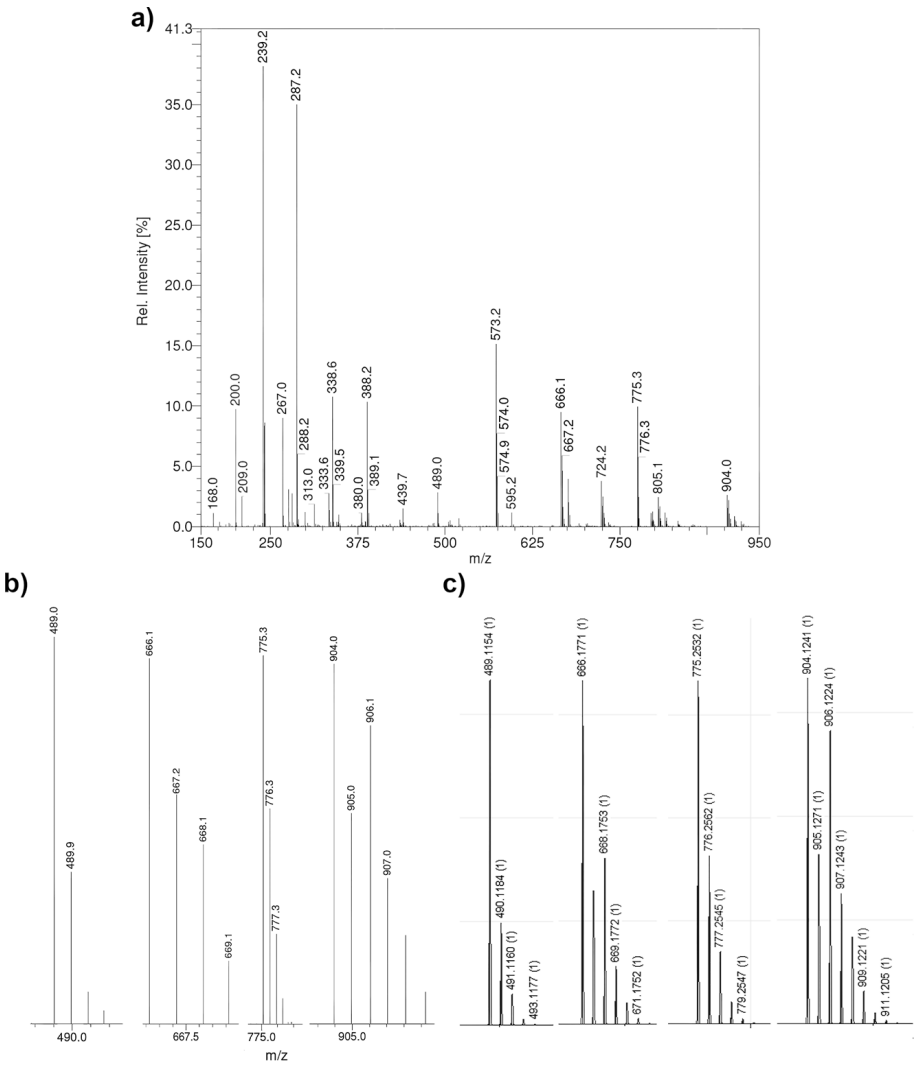

Figure AIV.19. ESI−MS spectrum of a) the reaction of Hquin, K_2CO_3, and *in situ* formed $[Co_2(L^3SSL^3)(Cl)_4]$ dissolved in methanol; b) the experimental isotopic distribution; c) simulated isotopic distribution spectra. ESI−MS found (calcd.) for $[Co(L^3S)(quin)]^+$ *m/z* 489.0 (489.1), for $[Co(quin)_2(MeCN)]^+$ *m/z* 387.9 (388.0), for $[L^3SSL^3 + H^+]^+$ *m/z* 573.2 (573.3), for $[L^3SSL^3 + 2H^+]^{2+}$ *m/z* 287.2 (287.2), for $[L^3SSL^3 + Co + Cl]^+$ *m/z* 666.1 (666.2), for $[L^3SSL^3 + Co + quin]^+$ *m/z* 775.3 (775.3), and for $[Co_2(L^3SSL^3)(Cl)_2(quin)]^+$ *m/z* 904.0 (904.1).

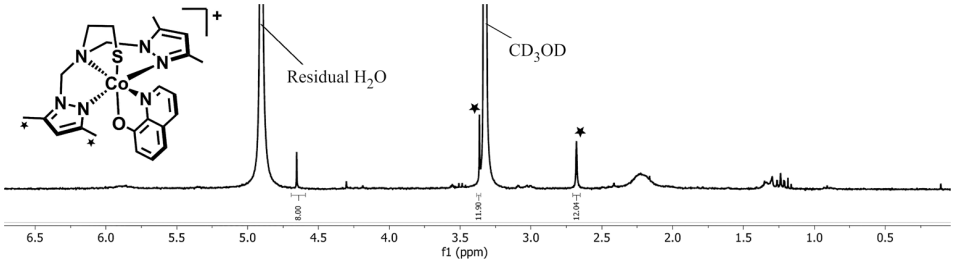

Figure AIV.20. ^{1}H-NMR spectrum of the brown powder of presumably [Co($L^{mpz}S$)(quin)]Br dissolved in $MeOD_4$. The aromatic region contains no signal.

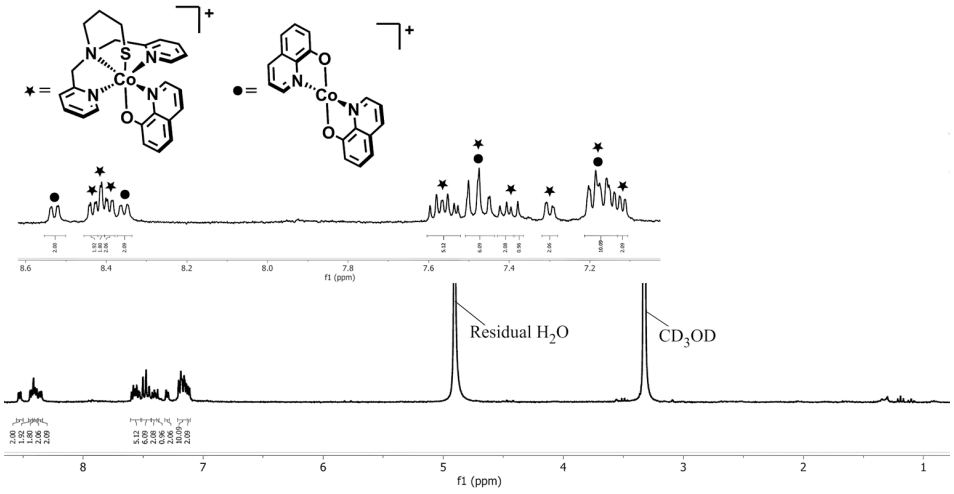

Figure AIV.21. ^{1}H-NMR spectrum of the brown powder of presumably [Co(L^PS)(quin)]Cl dissolved in $MeOD_4$. Inset shows the peaks in the aromatic region (between 7.0 – 8.6 ppm). The peaks assigned are for the species $[Co(L^PS)(quin)]^+$ and $[Co(quin)_2]^+$. However, the aliphatic peaks of the ligand L^PS are missing.

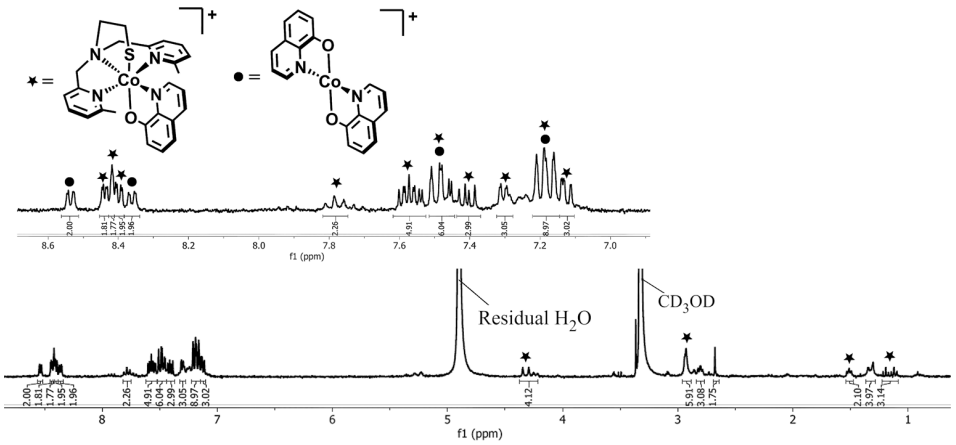

Figure AIV.22. ^{1}H-NMR spectrum of the brown powder of presumably [Co(L^3S)(quin)]Cl dissolved in $MeOD_4$. Inset shows the peaks in the aromatic region (between 7.0 – 8.6 ppm). The peaks assigned are for the species $[Co(L^3S)(quin)]^+$ and $[Co(quin)_2]^+$.

Table AIV.1. Crystallographic data for compound [$\mathbf{1}_{NCS}$] and [$\mathbf{1}_{Br}$].

	[$\mathbf{1}_{NCS}$]	[$\mathbf{1}_{Br}$]
Chemical formula	$C_{32}H_{44}Co_2N_{14}S_6 \cdot 2(C_2H_3N)$	$C_{28}H_{44}Br_4Co_2N_{10}S_2$
M_r	1017.14	1022.35
Crystal system	Monoclinic	Triclinic
Space group	*C*2/*c*	*P*-1
Cell lengths (*a, b, c*) (Å)	27.4033 (3), 10.05127 (11), 19.6772 (3)	8.6620 (3), 14.5167 (4), 15.3806 (4)
Cell angles (α, β, γ) (°)	90, 101.5415 (11), 90	82.892 (2), 82.030 (2), 89.653 (2)
Cell volume (Å^3)	5310.26 (12)	1900.49 (10)
Z	4	2
μ (mm^{-1})	7.43	5.22
Crystal size (mm)	0.38 × 0.28 × 0.22	0.14 × 0.07 × 0.04
Temperature (K)	110	110
Diffractometer	SuperNova, Dual, Cu at zero, Atlas detector	SuperNova, Dual, Cu at zero, Atlas detector
Radiation type	Cu *K*α	Mo *K*α
T_{min}, T_{max}	0.180, 0.396	0.632, 0.976
No. of measured, independent and observed [$I > 2\sigma(I)$] reflections	21714, 5193, 4734	32103, 7468, 6234
R_{int}	0.033	0.039
$(\sin \theta/\lambda)_{max}$ (Å^{-1})	0.616	0.617
$R[F^2 > 2\sigma(F^2)]$, $wR(F^2)$, S	0.035, 0.090, 1.04	0.038, 0.094, 1.03
No. of reflections	5193	7468
No. of parameters	276	423
H-atom treatment	H-atom parameters constrained	H-atom parameters constrained
$\Delta\rho_{max}$, $\Delta\rho_{min}$ (e Å^{-3})	0.45, -0.40	2.45, -1.37

Table AIV.2. Crystallographic data for compound [$\mathbf{2}_{NCS}$] and [$\mathbf{3}_{Cl}$].

	[**2**]	[**3**]
Chemical formula	$C_{34}H_{36}Co_2N_{10}S_6$	$C_{32}H_{40}Cl_4Co_2N_6S_2 \cdot 2(C_2H_3N)$
M_r	894.95	914.59
Crystal system	Monoclinic	Monoclinic
Space group	$P2_1/c$	$I2/a$
Cell lengths (*a, b, c*) (Å)	13.3213 (3), 11.5322 (3), 26.3107 (7)	15.3973 (3), 8.62095 (19), 31.1728 (6)
Cell angles (α, β, γ) (°)	90, 98.684 (2), 90	90, 97.3686 (19), 90
Cell volume (Å^3)	3995.62 (18)	4103.69 (15)
Z	4	4
μ (mm^{-1})	1.18	1.21
Crystal size (mm)	0.20 × 0.16 × 0.07	0.32 × 0.09 × 0.06
Temperature (K)	110	110
Diffractometer	SuperNova, Dual, Cu at zero, Atlas detector	SuperNova, Dual, Cu at zero, Atlas detector
Radiation type	Mo *K*α	Mo *K*α
T_{min}, T_{max}	0.645, 1.000	0.613, 1.000
No. of measured, independent and observed [$I > 2\sigma(I)$] reflections	47666, 9172, 7483	36703, 4706, 4209
R_{int}	0.037	0.031
$(\sin \theta/\lambda)_{max}$ (Å^{-1})	0.650	0.650
$R[F^2 > 2\sigma(F^2)]$, $wR(F^2)$, S	0.037, 0.094, 1.06	0.029, 0.075, 1.06
No. of reflections	9172	4706
No. of parameters	469	313
No. of restraints	-	171
H-atom treatment	H-atom parameters constrained	H-atom parameters constrained
$\Delta\rho_{max}$, $\Delta\rho_{min}$ (e Å^{-3})	0.74, -0.56	0.75, -0.30

Table AIV.3. Complete bond distances and bond angles in [**1**$_{\mathbf{Br}}$].

Atoms	Distance (Å)	Atoms	Bond angles (º)	Atoms	Bond angles (º)
Co1−S1	2.6084(12)	S1−Co1−N1	81.46(9)	N2−Co2−N32	74.37(13)
Co1–N1	2.264(3)	S1−Co1−N12	91.93(10)	N2−Co2−N42	74.51(13)
Co1–N12	2.129(3)	S1−Co1−N22	76.37(9)	N2−Co2−Br3	88.32(9)
Co1–N22	2.165(3)	S1−Co1−Br1	170.98(3)	N2−Co2−Br4	173.84(9)
Co1−Br1	2.4860(7)	S1−Co1−Br2	88.11(3)	Br4−Co2−N32	101.20(10)
Co1−Br2	2.5299(7)	Br1−Co1−N1	93.23(9)	Br4−Co2−N42	103.85(10)
Co2–N2	2.378(4)	Br1−Co1−N12	93.77(10)	Br4−Co2−Br3	97.83(3)
Co2–N32	2.072(4)	Br1−Co1−N22	95.31(9)	N32−Co2−N42	113.02(15)
Co2–N42	2.060(4)	Br1−Co1−Br2	97.18(2)	N32−Co2−Br3	129.64(12)
Co2−Br3	2.4242(7)	N1−Co1−N12	75.34(12)	N42−Co2−Br3	106.78(10)
Co2−Br4	2.4419(8)	N1−Co1−N22	75.77(12)		
S1−S2	2.0454(14)	N1−Co1−Br2	169.56(9)		
Co2−S2	6.090(1)	N12−Co1−N22	150.12(13)		

Table AIV.4. Complete bond distances and bond angles in [**1**$_{\mathbf{NCS}}$].

Atoms	Distance (Å)	Atoms	Bond angles (º)
Co1–N1	2.3701(17)	N1−Co1−N12	74.71(6)
Co1–N12	2.0444(17)	N1−Co1−N22	74.79(6)
Co1–N22	2.0400(17)	N1−Co1−N3	87.66(7)
Co1–N3	1.9788(18)	N1−Co1−N4	174.40(7)
Co1–N4	1.9952(19)	N4−Co1−N12	102.43(8)
S1–S1	2.0396(10)	N4−Co1−N22	102.70(7)
Co1–S1	6.0600(7)	N4−Co1−N3	97.94(8)
Co1–Co1	11.6906(6)	N3−Co1−N12	119.70(7)
		N3−Co1−N22	112.80(7)
		N12−Co1−N22	116.76(7)

Table AIV.5. Complete bond distances and bond angles in [**2**$_{\mathbf{NCS}}$].

Atoms	Distance (Å)	Atoms	Bond angles (º)	Atoms	Bond angles (º)
Co1–N1	2.2785(19)	N1−Co1−N11	77.09(7)	N2−Co2−N31	77.37(7)
Co1–N11	2.0661(19)	N1−Co1−N21	77.60(7)	N2−Co2−N41	78.38(8)
Co1–N21	2.0530(19)	N1−Co1−N51	174.26(8)	N2−Co2−N71	174.77(8)
Co1−N51	2.018(2)	N1−Co1−N61	87.42(8)	N2−Co2−N81	89.66(8)
Co1−N61	1.990(2)	N51−Co1−N11	99.20(8)	N71−Co2−N31	101.27(9)
Co2–N2	2.2337(19)	N51−Co1−N21	100.04(8)	N71−Co2−N41	97.35(9)
Co2–N31	2.032(2)	N51−Co1−N61	98.11(9)	N71−Co2−N81	95.44(9)
Co2–N41	2.0509(19)	N61−Co1−N11	113.19(9)	N81−Co2−N31	116.85(8)
Co2−N71	1.995(2)	N61−Co1−N21	127.31(8)	N81−Co2−N41	130.82(8)
Co2−N81	1.993(2)	N11−Co1−N21	112.01(7)	N31−Co2−N41	106.76(8)
S1−S2	2.0272(9)				
Co1−S1	6.2951(7)				
Co2−S2	5.6117(8)				
Co1−Co2	7.0894(7)				

Table AIV.6. Complete bond distances and bond angles in [**3**$_{Cl}$].

Atoms	Distance (Å)	Atoms	Bond angles (º)
Co1–N1	2.1406(14)	N1−Co1−N11	79.18(6)
Co1–N11	2.1631(14)	N1−Co1−N21	78.41(6)
Co1–N21	2.1918(15)	N1−Co1−Cl1	112.91(4)
Co1−Cl1	2.3235(5)	N1−Co1−Cl2	123.28(4)
Co1−Cl2	2.2976(5)	N21−Co1−N11	157.28(6)
S1−S1	2.0311(12)	N21−Co1−Cl1	95.81(4)
Co1−S1	4.8457(9)	N21−Co1−Cl2	93.52(4)
		N11−Co1−Cl1	96.29(4)
		N11−Co1−Cl2	95.63(4)
		Cl1−Co1−Cl2	123.78(2)